Review article: RE-SiAlON α/β - composites. Formation, thermal stability, phase relationships, reaction densification

(Artigo revisão: Compósitos TR α/β SiAlON. Formação, estabilidade térmica, relações de fases, densificação por reação)

V. A. Izhevskiy[1], L. A. Gênova, J. C. Bressiani
Instituto de Pesquisas Energéticas e Nucleares, CNEN/SP
C.P. 11049, Pinheiros, 05422-970, S. Paulo, SP, Brazil.

Abstract

In view of the considerable progress that has been made over the last several years on the fundamental understanding of phase relationships, microstructural design, and tailoring of properties for specific applications of rare-earth doped *SiAlONs*, a clear review of current understanding of the basic regularities lying behind the processes that take place during sintering of *SiAlONs* is timely. Alternative secondary phase development, mechanism and full reversibility of the $\alpha \leftrightarrow \beta$ transformation in relation with the phase assemblage evolution are elucidated. Reaction sintering of multicomponent *SiAlONs* is considered with regard of wetting behavior of silicate liquid phases formed on heating. Regularities of *SiAlON's* behavior and stability are tentatively explained in terms of RE-element ionic radii and acid/base reaction principle.

Keywords: SiAlON, phase transformation, structure evolution, N-melilite, reaction sintering

Resumo

Em vista do considerável progresso obtido nos últimos anos quanto à relação entre fases, o design microestrutural e a otimização de propriedades para aplicações específicas de SiAlONs dopados com elementos de terras-raras, se faz necessário uma clara revisão dos mecanismos envolvidos nos processos que ocorrem durante a sinterização dos SiAlONs. O desenvolvimento de segundas fases alternativas, os mecanismos e a completa reversibilidade da transformação $\alpha \leftrightarrow \beta$, em relação ao conjunto das fases são elucidados. Sinterização por reação de SiAlONs multi-componentes é analisada em relação à molhabilidade da fase líquida a base de silicato formada no aquecimento. Propõe-se uma explicação para a regularidade e estabilidade do comportamento dos SiAlONs em termos do raio iônico dos elementos de terras-raras e do princípio de reação ácido/base.

Palavras-chave: SiAlON, transformação de fases, evolução estrutural, N-melilita, sinterização por reação

INTRODUCTION

SiAlONs is a general name for a large family of the so-called ceramic alloys based on silicon nitride. Initially, they were discovered in the early 70-ies [1-3] and were developed actively since. The peak of activities in *SiAlON* research belongs to the 80-ies in which time fully dense polycrystalline bodies were prepared by pressureless sintering techniques. Profound understanding of basic regularities of the interrelation between the starting powder's properties, processing parameters and the properties of consolidated materials was achieved. The majority of the *SiAlON* phases were investigated and characterized. The latter applies to $\beta-SiAlON$, $\alpha-SiAlON$, *AlN* polytypoid phases, *O'-SiAlON*, as well as to a variety of crystalline secondary phases, mostly silicates, alumosilicates, and oxynitrides. Nitrogen-rich glasses were also thoroughly investigated. Although the initial goal of creating a single-phase silicon nitride based ceramics without any intergranular amorphous phases due to the transient liquid phase sintering was not achieved, *SiAlON* ceramics became one of the commercially produced high-tech ceramic materials.

There are two *SiAlON* phases that are of interest as engineering ceramics, $\beta-SiAlON$ and $\alpha-SiAlON$, which are solid solutions based on $\beta-$ and $\alpha-Si_3N_4$ structural modifications, respectively. $\beta-SiAlON$ is formed by simultaneous equivalent substitution of *Al-O* for *Si-N* and has most commonly been described by the formula $Si_{6-z}Al_zO_zN_{8-z}$. In this formula z can be varied continuously from zero to about 4.2 [4-6]. The homogeneity region of $\beta-SiAlON$ extends along the Si_3N_4-$(Al_2O_3$-$AlN)$ line. The unit cell contains two Si_3N_4 units. The $\alpha-SiAlON$ phase region has a fairly limited two-dimensional extension in the plane $Si_3N_4\frac{4}{3}(Al_2O_3 \cdot AlN) - MeN \cdot 3AlN$ of the *Me-Si-Al-O-N* phase diagram, the $\beta-SiAlON$ thus falling on one border of the plane mentioned. Of special interest are the *Me-Si-Al-O-N* systems where

[1] *Invited scientist, on leave from the Institute for Problems of Material Science, National Academy of Sciences of Ukraine, Kiev, Ukraine.*

the $\alpha-SiAlON$ phase is stabilized by the added *Me* ion, where *Me* is *Li*, *Mg*, *Ca*, *Y*, and the rare-earth metals except *La*, *Ce*, *Pr*, and *Eu* [7-9]. The $\alpha-SiAlON$ unit cell content, comprising four Si_3N_4 units, can be given in the general formula $Me_mSi_{12-(pm+n)}Al_{(pm+n)}O_nN_{16-n}$ for a metal ion Me^{p+}. Two substitution mechanisms may act; the first is similar to that of $\beta-SiAlON$ with *n (Si+N)* being replaced by *n (Al+O)*. The second mechanism is further replacement of $pmSi^{4+}$ by $pmAl^{3+}$, the electron balance being retained by incorporation of mMe^{p+} into the $\alpha-$phase structure.

$\alpha-SiAlON$ was most extensively studied in the *Y-Si-Al-O-N* system, where the two-dimensional phase field extension can be expressed as $Y_xSi_{3-(3x+n)}Al_{(3x+n)}O_nN_{4-n}$, with $0.08 < x < 0.17$ and $0.13 < n < 0.31$ [8, 10-13]. The lower solubility limit is located at $x \approx 0.08$ and *0.20* for cations with the radius of *0.095* to *0.1 nm*, and significantly higher, $x = 0.25$, for small cations such as ytterbium with a radius of $\approx 0{,}085$ *nm* [14]. It was also shown that by changing the overall composition in the *Y-SiAlON* system, $(\alpha+\beta)-SiAlON$ ceramics can be prepared with a varying $\alpha-SiAlON$: $\beta-SiAlON$ phase ratio [15, 16]. $\alpha-SiAlON$ always appears as equiaxed grains in the microstructure of the material, while $\beta-SiAlON$ forms elongated grains with an aspect ratio of 4 to 10. Hardness increases markedly with increasing $\alpha-SiAlON$ phase content, whereas the fracture toughness decreases. High $\alpha-SiAlON$ content also improves oxidation resistance of the material and the thermal shock resistance. It is also evident from its chemical composition that $\alpha-SiAlON$ offers possibility of reducing the amount of residual glassy grain-boundary phase by incorporating constituents of sintering aids into the crystal structure, which otherwise will be present as substantial amounts of residual glassy phase and deteriorate the high temperature performance of the material. Thus, $\alpha-SiAlON$ enables the preparation of the practically glass-free *SiAlON* composites, which may become interesting candidates for high-temperature structural and engineering applications.

The possibility of varying the *a-* $SiAlON:\beta-SiAlON$ phase ratio by slightly changing the overall composition was shown to open many possibilities to prepare *Y-SiAlON* ceramics with desired properties. This is of the utmost importance in connection with tailoring the properties for specific applications. Other ways of changing properties of *SiAlON* ceramics by means of replacing Y_2O_3 by other RE-oxide additives were also investigated [17]. Precisely this direction of research lead to discovery of the full reversibility of the $\alpha \Leftrightarrow \beta$ transformation for certain phase assemblies under conditions of post-sintering heat treatment [18-20]. It has been observed that the $\alpha-SiAlON$ phase is less stable at low temperatures and decomposes into rare-earth-rich intergranular phase(s) and $\beta-SiAlON$ with a remarkably elongated crystal morphology. The extent of the transformation is more pronounced with increased heat-treatment temperature. The mechanism of the fully reversible $\alpha \Leftrightarrow \beta$ transformation was investigated by the same authors [21]. This transformation provides an excellent possibility for optimizing phase content and microstructure without further additions of oxides and nitrides merely by heat treatment at appropriately chosen temperatures. In this way premeditated values of hardness, strength and toughness can be achieved from a single starting composition, which opens new perspectives for their successful application.

The objective of the present review, therefore, is to provide a comprehensive overall view of the new developments in *SiAlON*s that will facilitate advances of this subject, and allow areas for further study to be more clearly identified. The review will cover such important issues as thermal stability of different *RE*-doped $(\alpha-\beta)-SiAlON$ composites, phase relationships in this systems, alternative secondary phases for *SiAlON* ceramics, and mechanisms of reversible $\alpha \Leftrightarrow \beta$ transformation.

Occurrence of nitrogen melilite and nitrogen woehlerite solid solutions containing aluminum

Nitrogen melilite and woehlerite phases have been recently closely re-evaluated as the candidates for alternative secondary phases in Si_3N_4 based ceramics after the Al-containing solid solutions of this phases were discovered and investigated [22-25]. Nitrogen-containing (or *N*-) melilites and nitrogen-containing (or *N*-) woehlerites, the latter also known as *J*-phase, were discovered relatively early in the course of silicon nitride development and at the time were considered as undesirable secondary phases due to their poor oxidation resistance at temperature between 900 and 1100 °C [26]. Under such conditions they oxidize rapidly to crystobalite and $y-RE_2Si_2O_7$ with a ~30% increase in specific

Table 1 - Compilation of experimental data on the formation of N-melilite in different systems [33].

Cation	Ionic radius r_R^{3+} (Å)[a]	$r_R^{3+} : r_0^{2+}$	Al-free N-melilite formation	Formation of M' (R)	Maximum Al solubility in M'(R)
La^{3+}	1.016	0.77	Does not form	No study	Experimental data currently unavailable
Nd^{3+}	0.995	0.75	Observed	Observed	x = ~1.0
Sm^{3+}	0.964	0.73	Observed	Observed	x = ~1.0
Dy^{3+}	0.908	0.69	Observed	Observed	x = ~0.7
Y^{3+}	0.893	0.68	Observed (not at 1500 °C)	Observed	x = ~0.7
Yb^{3+}	0.858	0.65	Does not form	No study	Experimental data currently unavailable

volume, and this results in catastrophic cracking and total failure of material. N-melilites have the general formula $R_2Si_3O_3N_4$ (where *R*= yttrium or rare earth metal) and occur as an intermediate phase during sintering of a number of Si_3N_4-based ceramics. In particular, *N*-melilite is located in the phase compatibility regions of $\alpha-(\alpha-\beta)-SiAlONs$, which in theory can produce a good microstructure of SiAlONs N-melilite as the only secondary phase. *N*-melilite *(M(R))*, has a tetragonal structure that is built up of an infinite linkage of corner-sharing $Si(O,N)_4$ units in tetrahedral sheets perpendicular to the [001] direction. Sandwiched between these sheets are Y^{3+} or rare earth Ln^{3+} ions which hold the silicon oxynitride layers together [27]. The structure of *N*-woehlerite, or *J*-phase, is monoclinic and contains either $Si_2O_5N_2$ or Si_2O_6N ditetrahedral units containing *N* in the bridging position and arranged lengthwise along the *a*-axis. These units are linked by *RE* polyhedra.

Both phases are very stable refractory compounds and occur in almost all rare-earth systems [27]. With a very high melting point (~1900 ^{0}C for yttrium *N*-melilite [28]) and a composition close to a nitrogen-rich limit of the liquid region, these phases fulfill some of the ideal requirements for a grain boundary phase in *SiAlON* ceramics. However, the most important distinction of melilite-woehlerite type of secondary phases is that they do not have a eutectic with the matrix Si_3N_4 while the traditional oxide-base secondary phases have one unconditionally. This becomes absolutely obvious if one considers the phase diagram of *R-Si-(Al/O)-N* systems. A liquid region exists at high temperature, separating the Si_3N_4 corner and the plane of additive oxides and their compounds. In contrast, there is no liquid region between *M(R)/J(R)* and Si_3N_4. Although some liquid does form during initial heating because of the ternary eutectic of SiO_2, Al_2O_3, and R_2O_3, the liquid should be consumed largely by Si_3N_4 to form *M(R)* or *J(R)*. Thus, sintering of the latter composition is relatively difficult at the intermediate temperature for lack of liquid, but it improves drastically once the melting point of these phases is exceeded. Indeed, the lack of liquid at the intermediate temperature could be advantageous because it reduces the possibility of melt evaporation and massive powder relocation. Additionally, both melilite and woehlerite type phases crystallize readily on cooling directly from the liquid, which leads to quicker and much more complete crystallization as compared to any devitrification process.

The problem of catastrophic oxidation at intermediate temperatures is solved by formation of melilite and woehlerite based solid solutions containing aluminum. The general formulas of these solid solutions are $R_2Si_{3-x}Al_xO_{3+x}N_{4-x}$ and $R_4Si_{2-x}Al_xO_{7+x}N_{2-x}$, respectively. The solid solutions will be further referred to as *M'(R)* and *J'(R)*. In these phases, *Si-N* bonds are progressively being replaced by *Al-O* bonds as the Al solubility in the structure increases and this increase in oxygen content improves the oxidation stability.

Until now the regularities of solid solubility of aluminum in *M(R)* and *J(R)* were studied for the majority of *RE* elements (*Nd, Sm, Gd, Dy, Yb,* and *Y*) that are used in *SiAlON* production. It was unequivocally shown that the solid solubility range of *M'(R)* phases in respect of *Al* are determined by ionic radius of the *RE* element. With decreasing ionic radius the solubility limits in melilite solid solution decrease. For elements with large ionic radii, i. e., *R= Nd* and *Sm*, up to one *Si* can be replaced by *Al*. Consequently, yttrium melilite has the lowest observed aluminum solubility (*x= 0.6*) in rare earth elements melilite solid solutions [29]. The *N*-melilite phase is not stabilized by *Yb* and *La* [30-32], and therefore no study on these *M'(R)* was conducted. It was, however, shown that *Yb* forms *J'(R)* solid solution that can serve as an alternative secondary phase in this system. On the other hand, *La* forms only the *M'* phase with the highest substitution level (*x= 1*) while the *M'(La)* homogeneity range does not exist in *La-Si-Al-O-N* system. Here it must be specifically emphasized that phase pure *M(R)* or *M'(R)* were never formed neither in the form of a secondary phase, nor if synthesized separately according to stoichiometry. Appreciable amounts of *J'(R)*, *REAG* or other phases were present depending on the *RE* oxide used, the amount of *J'(R)* increasing with the decrease of the *RE* ionic radius. The results of the *M'(R)* solubility range determination systems are summarized in Table 1 [33].

The data on the correlation between the *x* value in *M'(R)* solid solution formula and the lattice parameters of *M'(R)* were determined for the majority of *RE* stabilizing elements [22, 29, 33]. Linear increase of the lattice parameters with increasing of the x values was observed for all systems investigated up to a certain *x* value for respective *M'(R)* phases. However, these *x* values do not necessarily represent true solubility limits as all samples contained additional phases, as it was mentioned earlier, some of them rare earth rich. It can, however, be noted that the *c/a* ratios are almost constant with increasing x-value for each *M'(R)* phase which indicates that the structural changes introduced when *Si-N* pairs are replaced by *Al-O* ones are isotropic in all *M'(R)* phases studied.

Since the nominal *x* value, i. e., the one determined by the powder mixture composition, was not relevant due to the multiphase nature of the synthesized materials, SEM-EDS studies have been used to estimate solubility limits of *Al* in various *M'(R)* phases. The maximum *Al* content, as determined in [29], were *x*=0.98, 0.9, 0.78, 0.71, and 0.57 for *R= Nd, Sm, Gd, Dy,* and *Y*, respectively. Thus, in *M' (Nd)* and *M'(Sm)* systems one *Si-N* pair per formula unit can be replaced by one *Al-O* pair in accordance with previous findings [22, 34, 35] while the true solubility limits in the *M'(Gd)* and *M' (Dy)* systems seem to be somewhat less (0.75) and even smaller in the *M' (Y)* system (0.60). These findings also confirm that the limit of *Al* solubility decreases with the ionic radii of the *RE* element [36]. It was also shown, that the substitution of *Si-N* by *Al-O* in the *M(R)* structure produces a lattice expansion [29]. The fact that the maximum value of lattice expansion was found in the *M' (Nd)* system (1.66%) and the minimum one in the *M' (Y)* system (0.70%) further supports the conclusion that the investigated systems exhibit different solid solubility ranges.

A tentative attempt to rationalize the interrelation between the ionic radii of RE element and the solubility limits of different *M'(R)* phases was made in [33] and is based on the simple considerations regarding the structure of melilite-type phases. The projection of the yttrium melilite on (100) may be schematically represented as shown in Fig. 1. With non-bridging anions taking up positions on the apex of the tetrahedra each silicon oxynitride layer of the *N*-melilite structure possesses an overall negative charge that has to be balanced by the *RE* cations. These cations separate the silicon oxynitride layers by a finite distance. In systems with small cation sizes such as yttrium or dysprosium, the negatively charged layers are allowed to come relatively closer together and possibly create a repulsive force which can destabilize the melilite structure. A structurally unstable *M'(R)* phase may result in a low *Al* accommodation capability. However, the exact mechanism involved in this process is currently unknown.

One of the main issues of interest in regard of the properties of

the *M'(R)* phases is their behavior at high temperatures primarily in relation with densification of respective compositions. *Al*-free melilites tend to become unstable at temperatures exceeding 1800 °C. Melting of melilites is thought to be impossible because the edge of the liquid region in the four component *R-Si-O-N* plane does not reach as far as the melilite composition (i. e., 67 eq.% nitrogen). Instead, the melilite phases are believed to decompose with significant loss of nitrogen, resulting in the formation of *J* phase. For *M'(R)*, stability at high temperature is determined by two factors. With increasing aluminum content, the limiting composition of *M'(R)* gradually moves towards the liquid region, and at the same time the liquid region can accommodate a higher nitrogen concentration with increasing temperature, approaching the terminal composition of *M'(R)*. Current preparative evidence suggests that the liquid region eventually reaches the *M'(R)* composition, and *M'(R)* melts [22]. This generates large amounts of liquid which, in combination with *Si*, *N*, and other components, promotes the precipitation of α*-SiAlON* phase and accelerates the final densification. This effect has been widely observed in several *SiAlON* systems [34, 37].

It is clear that the melting temperature of *M'(R)* varies in different systems according to the densifying cation, but a low melting temperature for *M'(R)* is a key factor in the preparation of dense α- and (α+β)*-SiAlON* ceramics. According to [22] the *M'(Sm)* melts at about cooling 1700 °C and on cooling at normal furnace cooling rate *M'(Sm)* reprecipitates, suggesting that any liquid with *M'(R)* composition does not form a glass. Although it has not yet been confirmed that dissolution of aluminum in *M(R)* actually lowers the melting temperature of these phases, but the closeness of the *M'(R)* composition to the liquid-forming region certainly dominates the behavior of *M'(R)* phases at high temperatures. As it will be discussed further, the high temperature behavior of *M'(R)* phases plays an important role in the reversible $\alpha \Leftrightarrow \beta$ transformation in *SiAlON* ceramics.

Another important factor in designing and processing of various silicon nitride based materials, (α-β)*-SiAlONs* in particular, are the phase relations of *M'(R)* with the neighboring phases in different *M-Si-Al-O-N* systems. The most thorough and systematic research of this subject was accomplished in [38, 39]. This research covered the majority of *RE*-metal oxides (*RE= La, Gd, Dy, Er, Y, Nd, Sm,* and *Yb*) that are used as sintering aids in complex *SiAlON* systems. Firstly, it was shown that the nominal compositions of *N*-melilite do not form a single-phase material for neither of the RE elements investigated. Moreover, it was unequivocally shown that *M(R)* is not formed with *La*, which, depending on the synthesis conditions, forms a mixture of *K*-phase ($La_2O_3 \cdot Si_2N_2O$) and *1:2* phase ($La_2O_3 \cdot 2Si_3N_4$) in this or that proportion. The results of the attempts of *M(R)* synthesis with different RE elements are listed in Table 2.

The tendency for forming different components in high-temperature synthesis can be rationalized using the concept of acid-base reactions [40]. Silicon nitride may be considered as more acidic than Si_2N_2O, which enters the compositions of *J* ($2R_2O_3 \cdot Si_2N_2O$) and *K* ($R_2O_3 \cdot Si_2N_2O$) phases, formed by different *RE* elements as "impurity" or additional phases (see Table 2), and light rare earth oxides as more basic than heavy rare earth oxides. The various minor phases formed in the presence of melilite then can be viewed as the product of the following reactions:

1:2 phase	$La_2O_3 \cdot 2Si_3N_4$	(strong base / strong acid)
K(R) phase	$La_2O_3 \cdot Si_2N_2O$	(strong base / weak acid)
J(R) phase	$2Y_2O_3 \cdot Si_2N_2O$	(weak base / weak acid)

For example, as the basicity of R_2O_3 decreases with decreasing ionic radius, it prefers to react with a weak acid to form J phase rather than *K* or *1:2* phase. It is also interesting to note that the molar ratio of base to acid in *K(R)* and *J(R)* increases from 1:1 to

Table 2 - Reactions and phase formation in $R_2Si_3O_3N_4$ compositions [39].

Rare-earth element, R	Reaction temperature (°C)/time(h)	Appearance	Phase analysis by XRD	M(R) lattice parameter (Å) a	c
Lanthanum	1650/2 (Sintering)	White	K, 1:2		
	1550/1.5 (HP)	Gray	K, 1:2		
	1600/1.5 (HP)	Gray	K, 1:2		
	1650/1.5 (HP)	Black	1:2, K		
Neodymium	1650/2 (Sintering)	Blue	M, K (vw)	7.721	5.036
	1700/1.5(HP)	Blue	M, K (w)		
Samarium	1700/2 (Sintering)	White	M, K (vw)		
	1700/1.5 (HP)	Brown	M, K (vw)	7.695	4.991
Gadolinium	1700/2 (Sintering)	White	M, K (vw)	7.650	4.961
Dysprosium	1700/2 (Sintering)	White	M, J (w)	7.618	4.925
Europium	1700/2 (Sintering)	Pink	M, J, 2:1		
	1700/1.5 (HP)	Pink	M, J (mw)	7.585	4.896
Ytterbium	1700/2 (Sintering)	Black	M, J, 2:1		
	1700/1.5 (HP)	Black	M, J (mw)	7.563	4.876

mw - medium weak, w – weak, vw – very weak

2:1; this reflects the need for a larger amount of the weaker base to react with the same acid.

Interesting results and trends were discovered for *M'(R)* phases when an attempt was made to synthesize the nominal composition $R_2Si_2AlO_4N_3$. *M'(R)* solid solution was found in all cases except ytterbium (Table 3). Overall, the systematic trend of phase distribution discovered was very similar with the one for *M(R)*, with the minor phases favoring *K*-phase, in the case of lanthanum, and *J*-phase, in the case of heavy rare-earth elements. However, some differences were also discovered.

First, in the case of *La*, melilite solid solution was formed. This is in contrast with *Al*-free composition, which did not form *La*-melilite. The lattice parameters of *M' (La)* were larger than all of the other *M(R)* and *M'(R)* found so far ($a = 7.855$ Å and $c = 5.120$ Å). The composition of *M' (La)* was found to be $La_{1.98}Si_{1.82}Al_{0.96}O_{4.21}N_{3.08}$, i. e., essentially an $x = 1$ compound in the $R_2Si_{3-x}Al_xO_{3+x}N_{4-x}$ series. Similar compositional investigations revealed that the x value decreases monotonically with the atomic number of the *RE*-element. This can be interpreted as a size effect. From the interrelation between the ionic radii of *RE* elements and both x value and (cubic root of) unit cell volume, $(a^2c)^{1/3}$, from *M(R)* and *M'(R)* (Fig. 2) it is clear that the unit cell has expanded in *M'(R)* relative to *M(R)*. This is accompanied by the substitution of *Si-O* bond (bond length 1.62 Å) and *Si-N* bond (1.74 Å) by *Al-O* bond (1.75 Å). Apparently, in the case of lanthanum, which has a very large radius, only after maximal substitution, $x = 1$, is it possible to incorporate lanthanum into the melilite structure. In case of ytterbium, which has a very small radius in contrast, it is apparently stable only in the limit of smallest volume realizable at $x = 0$.

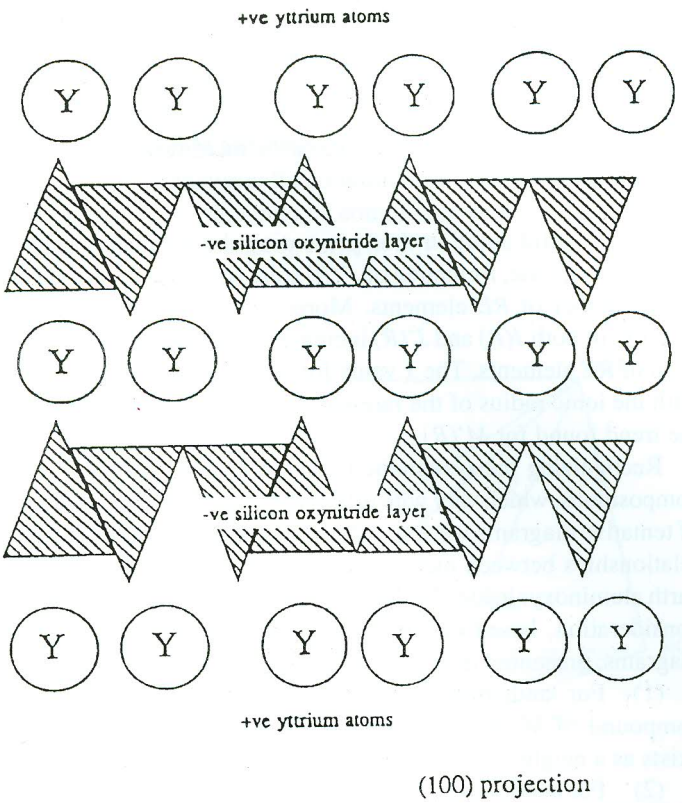

Figure 1: Schematic representation of the structure of yttrium N-melilite showing separation of the negatively charged silicon oxynitride layers by Y^{3+} cations [33].

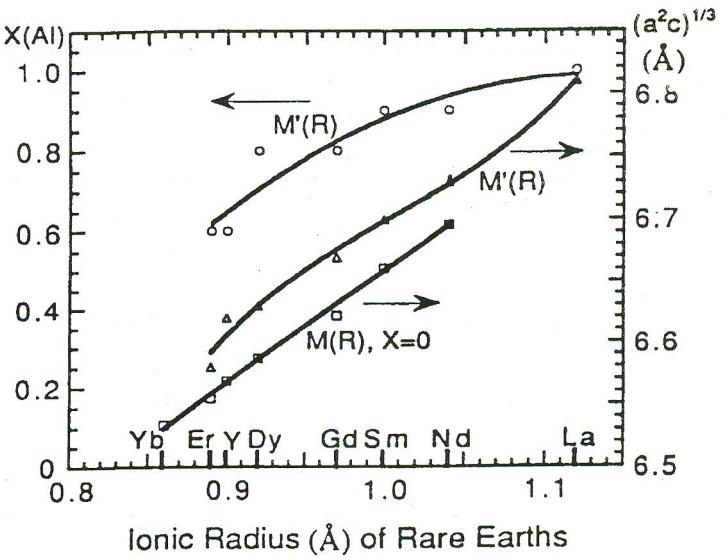

Figure 2: X(Al) atomic fraction in M'(R) and cell size as a function of ionic radii of rare-earth elements [39].

The lattice parameters of melilite and its solid solution obtained for different rare-earth elements at different x values can be correlated to each other, according to [39], by the following formula:

$$a(\text{Å}) = 6.795 + 0.892r + 0.045x$$

$$c(\text{Å}) = 4.121 + 0.874r + 0.033x$$

where r is the ionic radius (in angstroms) of the rare-earth ion using Ahrens scale. These formulas were obtained by a regression analysis of the experimental data on XRD-determined lattice parameters of *M(R)* and *M'(R)* formed by different *RE*-elements and can be used for identifying the composition of $R_2Si_{3-x}Al_xO_{3+x}N_{4-x}$ once the identity of the rare-earth element is known.

As to the two other phases, *K* and *J*, that were present in the synthesized samples the mechanism of formation and the trends of stability were also formulated in [39]. Formation of *K* phase was attributed to the reaction of R_2O_3 with the surface-oxidized Si_3N_4, forming Si_2N_2O. In the case of the aluminum-containing compositions, the oxidized nitride was supposed to be incorporated

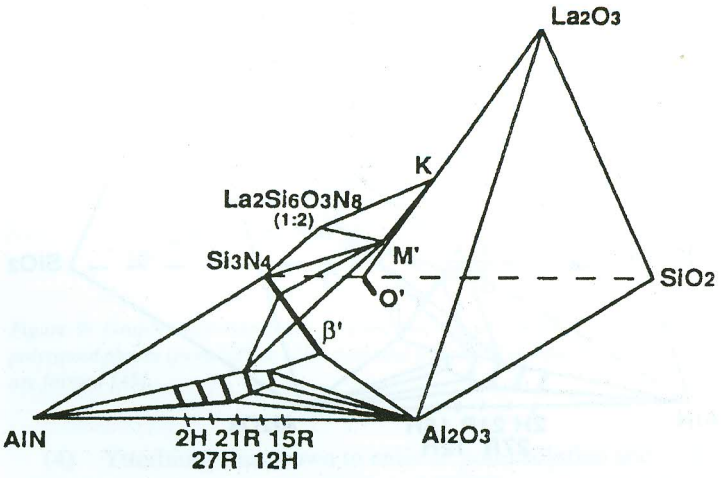

Figure 3: Phase relations of M'(La) with neighboring phases in La-Si-(Al/O)- N system [39].

Table 3 - Reactions and phase formation in $R_2Si_2AlO_4N_3$ compositions [39].

Rare-earth element, R	Reaction temperature (^{0}C)/time(h)	Appearance	Phase analysis by XRD	M(R) lattice parameter (Å)	
				a	c
Lanthanum	1650/2	Partly melted	1:2, K		
	1600/2	White, not dense	M', K, 1:2	7.855	5.120
	1550/1.5 (HP)	Gray	K, 1:2, M'		
Neodymium	1650/2	Purple	M'	7.766	5.055
Samarium	1650/2	Brown	M'	7.730	5.014
Gadolinium	1650/2	Gray	M'	7.689	4.993
Dysprosium	1650/2	Yellow	M', J' (vw)	7.655	4.955
Yttrium	1650/2	White	M', J' (w)	7.629	4.929
Europium	1650/2	Pink	M', J' (mw)	7.608	4.920
Ytterbium	1650/2	Black	J'		

mw - medium weak, w – weak, vw – very weak

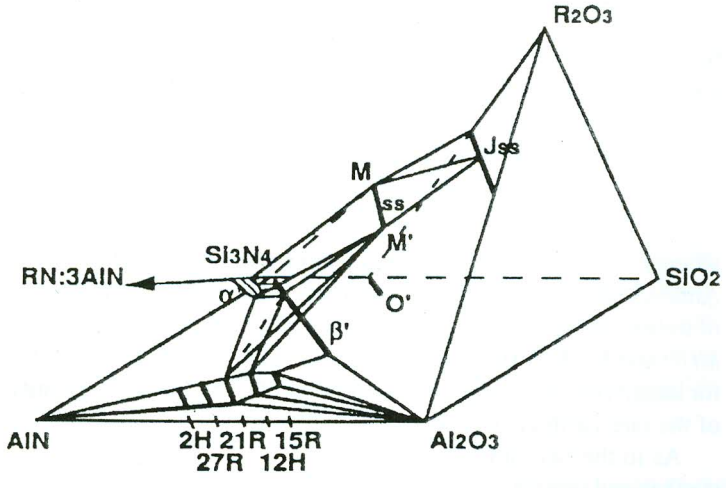

Figure 4: Phase relations of M'(La) with neighboring phases in R-Si-(Al/O)- N (R = Gd, Dy, Er, Y) system [39].

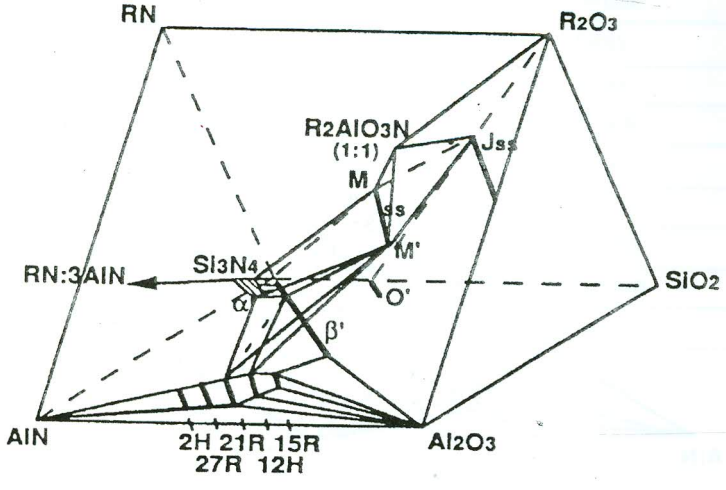

Figure 5: Phase relations of M'(La) with neighboring phases in R-Si-(Al/O)- N (R = Nd, Sm) system [39].

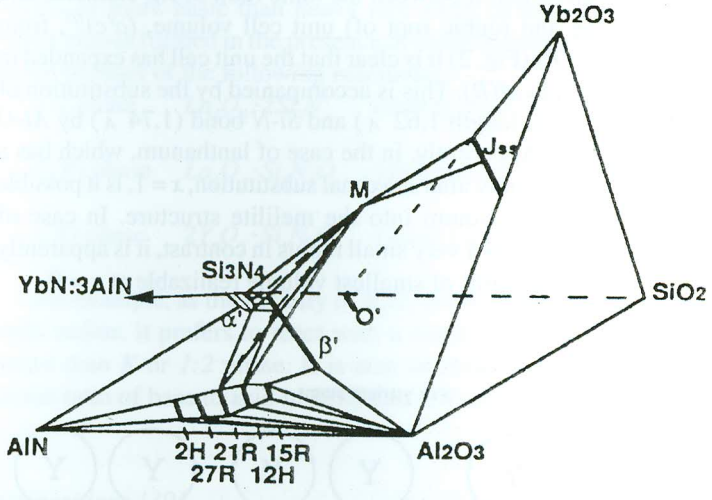

Figure 6: Phase relations of M'(La) with neighboring phases in Yb-Si-(Al/O)- N system [39].

into *M'(R)* solid solution thus preventing the formation of the *K* phase. For *J* phase, formation of *J'(R)* solid solutions was confirmed for a number of *RE* elements. Moreover, it was shown that the stability of both *J(R)* and *J'(R)* increases with the decrease of ionic radii of *RE* elements. The *x* value for *J'(R)* was shown to increase with the ionic radius of the rare-earth element, which is similar to the trend found for *M'(R)*.

Recognizing the systematic trends in *M'(R)*, *J'(R)*, *α'*, and *β'* compositions, which vary with different rare-earth elements, a series of tentative diagrams were suggested in [39] to delineate the phase relationships between melilite and neighboring phases. The rare-earth aluminoxynitride, R_2AlO_3N, denoted as 1:1, was included into consideration, based on the findings of [41]. Four prototypical diagrams, presented in Fig. 3-6, illustrate these relationships:

(1) For lanthanum, there is no *α'* solid solution; the $x = 1$ compound of *M'(R)* forms. In addition, $La_2Si_6O_3N_8$ (1:2 phase) exists as a neighboring phase (see Fig. 3);

(2) For neodymium and samarium, there is an extensive solid solution of both *α'* and *M'(R)*, but only *J* phase, not *J'(R)* solid solution, is compatible with *M'(R)*. In addition, R_2AlO_3N forms

Table 4 - Subsolidus compatibility tetrahedra in Si_3N_4-AlN-Al_2O_3-Y_2O_3 [45].

Al_2O_3-β_{60}-15R-YAG	Al_2O_3-15R-15R'-YAG
$Al_2O_3$15R'-12H'-YAG	Al_2O_3-12H'-21R'-YAG
Al_2O_3-21R'-AlN-YAG	15R-15R'-12H-12H'-YAG
12H-12H'-21R-21R'-YAG	21R-21R'-27R-27R'-YAG
27R-27R'-2H$^{\delta}$-2H$^{\delta}$'-YAG	2H-2H$^{\delta}$-AlN-YAG
21R'-27R'-AlN-YAG	27R'-2H$^{\delta}$'-AlN-YAG
21R-27R-YAG-J'(R)	27R-2H$^{\delta}$-YAG-J'(R)
2H$^{\delta}$-AlN-YAG-J'(R)	AlN-YAG-J'(R)-YAM
AlN-YAM-J-Y_2O_3	β_{60}-β_{25}-15R-YAG
β_{25}-15R-12H-YAG	β_{25}-β_{10}-12H-YAG
β_{10}-$\alpha\alpha$'-12H-YAG	α'-12H-21R-β_{10}
α'-21R-β_{10}-β_8	α'-21R-β_8-27R
α'-β_8-27R-β_2	α'-27R-β_5-2H$^{\delta}$
α'-β_5-2H$^{\delta}$-β_2	α'-2H$^{\delta}$-β_2-AlN
α'-β_2-AlN-Si_3N_4	α'-12H-21R-YAG
α'-21R-YAG- M	α'-21R-27R-M
α'-27R-2H$^{\delta}$-M	α'-2H-AlN-M
M-21R-YAG-J'(R)M-21R-27R-J'(R)	M-21R-27R-J'(R)
M-27R-2H$^{\delta}$-J'(R)	M-2H$^{\delta}$-AlN-J'(R)
M-AlN-J'(R)-J	

YAM = $2Y_2O_3 \cdot Al_2O_3$; J = $2Y_2O_3 \cdot Si_2N_2O$; J'(R) = $2Y_2O_3 \cdot Al_2O_3$-$Y_2O_3 \cdot Si_2N_2O$; M = $Si_3N_4 \cdot Y_2O_3$; 15R, 12H, 21R, 27R, 2H$^{\delta}$ are Si-rich terminals of AlN polytypoids; 15R', 12H', 21R', 27R', 2H$^{\delta}$' are Al-rich terminals of AlN polytypoids.

and is compatible with *M'(R)* and *J* (see Fig. 4). The compatibility of $RAlO_3$ (*R* = *Nd*, *Sm*) with *M'(R)* were not resolved. According to [39], *M'(R)* is compatible with $RAlO_3$, while according to [42] $SmAlO_3$ may be just a product that forms on cooling at some specific conditions and, in fact, is not compatible with *M'(R)*. In [39] only coexistence of *M'(R)*, R_2AlO_3N and *J* phase at 1550 °C was found.

(3) For gadolinium, dysprosium, europium, and yttrium, there was found an extensive solid solution of α', but the solid solution range of *M'(R)* was shown to be compatible with *M'(R)*, while the compound R_2AlO_3N failed to form in this case (see Fig. 5).

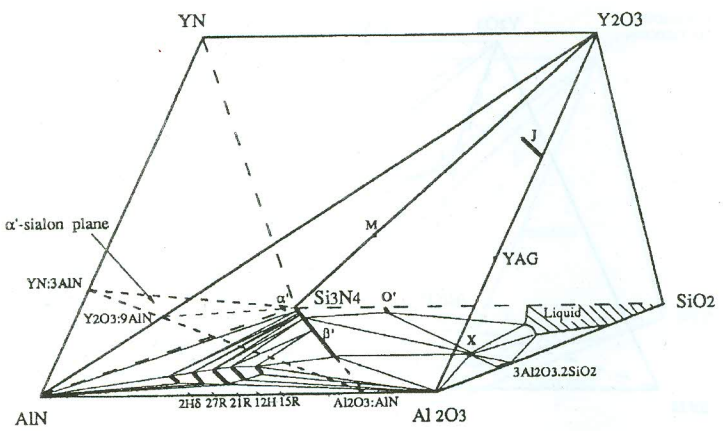

Figure 7: Representation of Y-Si-Al-O-N system showing phases occurring in the region bound by Si_3N_4, Y_2O_3, Al_2O_3, and AlN, and Si-Al-O-N behavior diagram at 1700 °C [45].

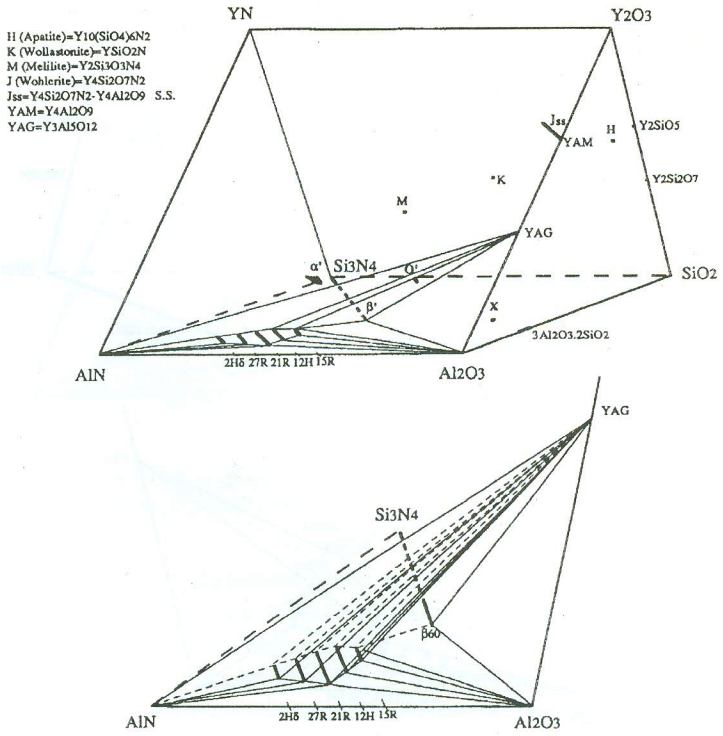

Figure 8: Graphic representation of compatibility of the YAG with polytypoid phases, AlN, and Al_2O_3, twelve compatibility tetrahedra are formed [45].

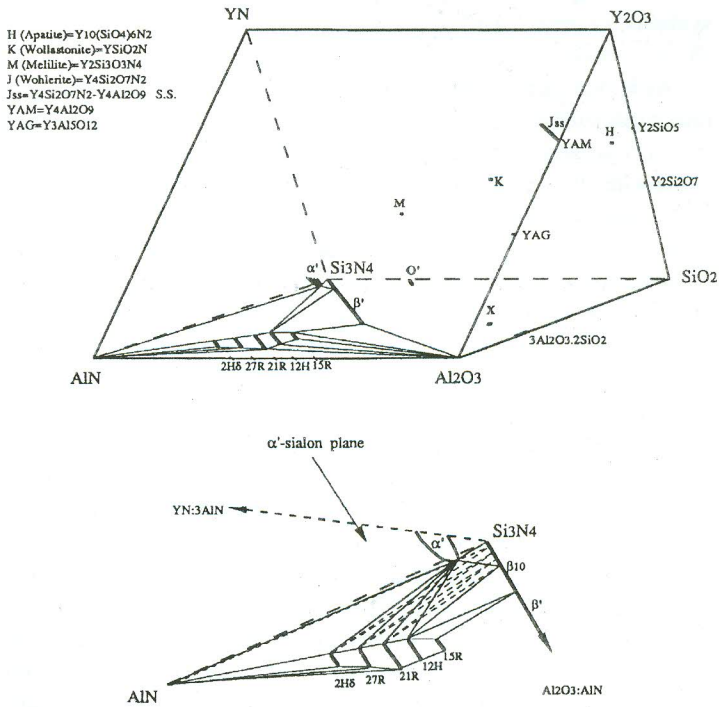

Figure 9: Graphic representation of compatibility of the $\alpha\alpha''$—SiAlON with polytypoid phases (from 2H$^{\delta\delta}$ to 12H), AlN, and $\beta\beta''$, eight compatibility tetrahedra are formed [45].

(4) Ytterbium was shown to enter α' solid solution and *J'(R)* solid solution. However, only *M(R)*, not *M'(R)*, was proven to form in this case (see Fig. 6).

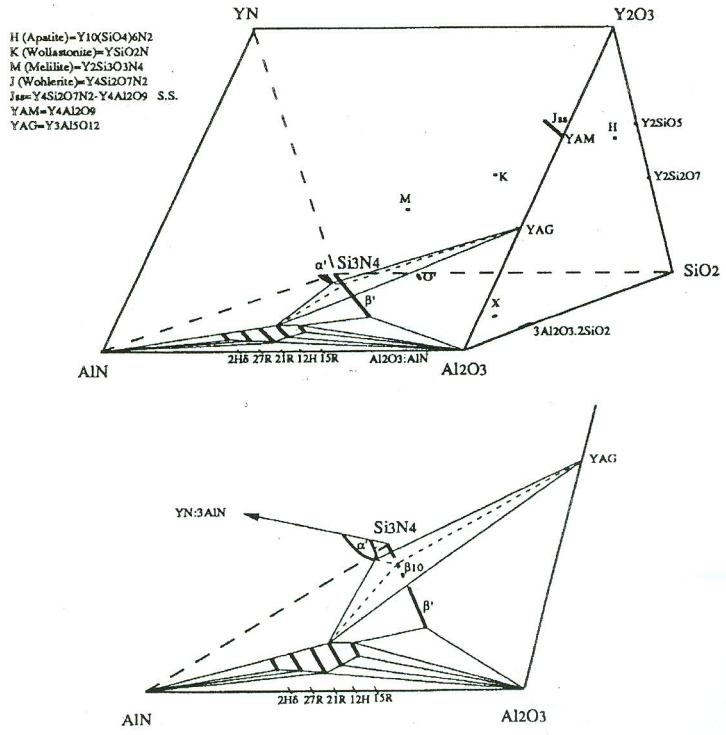

Figure 10:Compatibility tetrahedron α'–β_{10}–12H–YAG [45].

Subsolidus phase relationships in R_2O_3 – Si_3N_4 – AlN – Al_2O_3 systems

As it was already mentioned before, the importance of using rare earth oxides for the densification of silicon nitride ceramics was recognized in recent years. Not only are they very effective along with alumina for densification, either singly or in combination with yttria, but they can also be accommodated in the $\alpha-Si_3N_4$ lattice forming $\alpha-SiAlON$ ($\alpha-Si_3N_4$ solid solution with the composition $Ln_xSi_{12-(m+n)}Al_{m+n}OnN_{16-n}$, also designated as α'), thus providing the opportunity for decreasing the transient liquid phase content after sintering and hence reducing the amount of residual grain boundary glass. Therefore, phase relationships in *Ln-Si-Al-O-N* systems are of particular interest.

The most well investigated system is *Y-Si-Al-O-N* system. Most of the early work in this system has been restricted to the region bounded by $Si_3N_4-\beta-SiAlON-Al_2O_3-SiO_2$ and Y_2O_3, which does not include the solid solution $\alpha'-SiAlON$. *Huang at al.* reported the $\alpha-SiAlON$ formation in the system $Si_3N_4-AlN-Y_2O_3$ [43] and Si_3N_4–*AlN–rare earth oxide* [14]. The systems Si_3N_4–AlN–Y_2O_3 and $Si_3N_4-AlN:3AlN-Al_2O_3$: *AlN* have also been studied by the same authors [44]. Later, with the emergence of α'–*SiAlON*, information on the nitrogen-rich part of the *Si, Al, Y/N, O* became necessary and the investigations in this system were completed [45]. Thirty-nine compatibility tetrahedra had been established in the region $Si_3N_4-AlN-Al_2O_3-Y_2O_3$ (Table 4). The subsolidus phase relationships in the region $Si_3N_4-AlN-YN-Y_2O_3$ were also determined. Only one compound, $2YN:Si_3N_4$, was confirmed in the binary system Si_3N_4-YN contrary to the early results of Thompson [46] who reported the existence of three compounds: $6YN:Si_3N_4$, $2YN:Si_3N_4$, and $YN:Si_3N_4$. This contradiction could be explained by the purity of the *YN* used as a starting material, and in that case the X-ray diffraction lines of $2YN:Si_3N_4$ and $YN:Si_3N_4$ reported by Thompson may be regarded as a mixture of melilite ($Y_2Si_3O_3N_4$), *J* phase ($2Y_2O_3:Si_2N_2O$), and other oxygen-containing phases. The solubility limits of the α–*SiAlON* on the Si_3N_4–*YN:3AlN* join were determined to range from m=1.3 to m=2.4 in the formula $Y_{m/3}Si_{12-m}Al_mN_{16}$. No quinary compounds were found. Seven compatibility tetrahedra were established in the region $Si_3N_4-AlN-YN-Y_2O_3$ (Table 4).

Sixty eight compatibility tetrahedra were established in the system *Si, Al, Y/N, O*: thirty-nine in the region bounded by $Si_3N_4-SiO_2-AlN-Al_2O_3-Y_2O_3$, seven in the region bounded by $Si_3N_4-AlN-YN-Y_2O_3$, and twenty-two in region $Si_3N_4-\beta_{60}-Al_2O_3-SiO_2$ and Y_2O_3. All this data are graphically presented in Fig. 7-11.

Subsolidus phase relationship in $Ln_2O_3-Si_3N_4-AlN-Al_2O_3$ systems until now were thoroughly investigated for most of *RE* elements, although not in such a detailed and profound way as the *Y*–doped one. The determination of the whole system, represents a very large amount of work and most initial studies have restricted to the sub-systems *Ln-Si-O-N*, *Ln-Al-O-N* (*Ln = Ce, Pr, Nd* and *Sm*) and some planes involving α– and β–*SiAlON* [14, 34]. It is known that elements in the lanthanide (*Ln*) series are similar to yttrium in compound formation and phase relationships. Previous research on *Ln-Si-O-N* subsystems [47], indicates that the phase relationships are nearly the same as in the *Y-Si-O-N* system, but in *Ln-Al-O-N* systems [48] the phase relationships were shown to vary with atomic number of the rare earth element. The phase relationships in the systems with high *Z*-value of the rare earth element are similar to those in *Y-Al-O-N* [49]. In the systems *Ln-Al-O-N* (where *Ln = Ce*→ *Sm*) to nitrogen containing compounds exist – Ln_2AlO_3N and $Ln_{12}Al_{12}O_{18}N_2$ (magneto-plumbite, *MP* compound) – and no garnet phase occurs; instead the *1:1* aluminate phase becomes stable [48]. The Ln_2AlO_3N and *MP* compounds do not occur in those systems containing rare earth oxides with cations smaller than that of *Gd* [14, 48]. Therefore, in the five-component systems with the low Z-value rare earth elements, the phase relationships become slightly different from those in *Y-Si-Al-O-N*. In the oxygen-rich region where two five-component phases [50, 51] – *U*-phase ($Ln_3Si_{3-x}Al_{3+x}O_{12+x}N_{2-x}$) and *W*-phase ($Ln_4Si_9Al_5O_{10}N$) – exist, the former is stable for rare earth cations between *La* and *Dy* the latter stable only in *La, Ce* and *Nd* systems. None of the phases above occur in the *Y* system. The stability of *N-melilite*

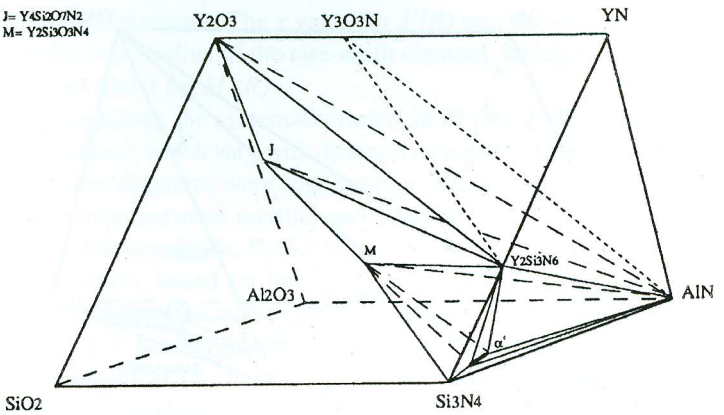

Figure 11: Subsolidus phase relationships in the region bound by Si_3N_4, AlN, YN, and Y_2O_3 [45].

Table 5 - Subsolidus compatibility tetrahedra in the systems Si_3N_4-AlN-Al_2O_3-Ln_2O_3 (Ln = Nd and Sm) [52].

Al_2O_3-β_{60}-15R-MP	Al_2O_3-15R-15R'-MP
$Al_2O_3$15R'-12H'-MP	Al_2O_3-12H'-21R'-MP
Al_2O_3-21R'-AlN-MP	15R-15R'-12H-12H'-MP
12H-12H'-21R-21R'-MP	21R-21R'-27R-27R'-MP
27R-27R'-2H$^{\delta}$-2H$^{\delta}$'-MP	2H$^{\delta}$-2H$^{\delta}$'-AlN-MP
21R'-27R'-AlN-MP	27R'-2H$^{\delta}$'-AlN-MP
AlN-2H$^{\delta}$-MP-$LnAlO_3$	2H$^{\delta}$-27R-MP-$LnAlO_3$
27R-21R-MP-$LnAlO_3$	21R-12H-MP-$LnAlO_3$
12H-15R-MP-$LnAlO_3$	β_{60}-15R-MP-$LnAlO_3$
β_{60}-Al_2O_3-MP-$LnAlO_3$	β_{60}-β_{25}-15R-$LnAlO_3$
β_{25}-15R-12H-$LnAlO_3$	β_{25}-β_{10}-12H-$LnAlO_3$
β_{10}-12H-$LnAlO_3$-M'	β_{10}-12H-21R-M'
α'-β_0-β_{10}-M'	α'-β_{10}-21R-M'
α'-β_{10}-β_8-21R	α'-β_8-21R-27R
α'-β_8-β_5- 27R	α'-β_5-27R-2H$^{\delta}$
α'-β_5-β_2-2H$^{\delta}$	α'-β_2-2H$^{\delta}$-AlN
α'-β_2-β_0 AlN	α'-AlN-2H$^{\delta}$-M'
α'-2H$^{\delta}$-27R-M'	α'-27R-21R-M'
M'-12H-21R-$LnAlO_3$	M'-21R-27R-$LnAlO_3$
M'-27R-2H$^{\delta}$-$LnAlO_3$	M'-2H$^{\delta}$-AlN-$LnAlO_3$
M'-AlN-$LnAlO_3$-J(R)	M'-AlN-J(R)-M
AlN-$LnAlO_3$-J(R)-Ln_2AlO_3N	$LnAlO_3$-J(R)-Ln_2AlO_3N-Ln_2O_3

MP = $LnAl_{12}O_{18}N$; M' = $Ln_2Si_{3-x}Al_xO_{3+x}N_{4-x}$; J(R) = $Ln_4Si_2O_7N_2$; 15R, 12H, 21R, 27R, 2H$^{\delta}$ are Si-rich terminals of AlN polytypoids; 15R', 12H', 21R', 27R', 2H$^{\delta}$' are Al-rich terminals of AlN polytypoids.

($Ln_2Si_{3-x}Al_xO_{3+x}N_{4-x}$) in different are earth systems was discussed in the previous section of this paper.

Most closely and most recently the subsolidus phase relationships were studied in *Nd* and *Sm* [52], and *Dy* [53] containing Ln_2O_3–Si_3N_4–AlN–Al_2O_3 systems. The attention paid to the former two elements is caused by the efforts to substitute *Y* by some cheaper *RE* elements in Si_3N_4–based ceramics without hindering the properties. *Dy* containing system was chosen because dysprosium

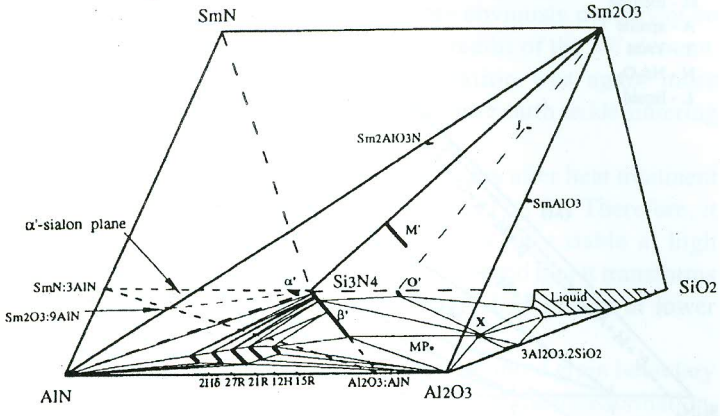

Figure 12: Representation of Sm(Nd)-Si-Al-O-N system showing phases occurring in the region bound by Si_3N_4, $Sm(Nd)_2O_3$, Al_2O_3, and AlN, and Si-Al-O-N behavior diagram at 1700 ^{0}C [52].

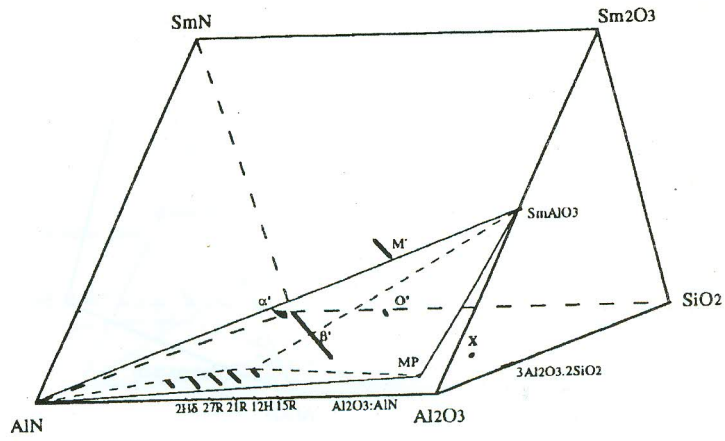

Figure 13: $Sm(Nd)_2O_3$ is compatible with all polytypoid phases (Si-rich terminal), AlN, and $Sm(Nd)Al_{12}O_{18}N$ (MP compounds) forming five compatibility tetrahedra [52].

is one of the central elements in the rare earth series: in this region, phase relationships in *Ln-Si-Al-O-N* systems are changing from those observed for the low-*Z* elements (*La, Nd, Sm*) to those observed for high-*Z* elements (*Er, Yb...* and *Y*). It was therefore interesting to find out whether these changes occur simultaneously or whether there is overlap in this region between the different phase relationships observed for the high-*Z* and low-*Z* rare earths.

According to [52], *Sm* has the same behavior as *Nd* in regard of phase formation, but it was noted that melting temperatures were lower in the samarium system and consequently, at a given temperature, the size of the liquid-forming region is larger. For both *Sm* and *Nd* systems 44 compatibility tetrahedra were established (Table 5). Some specific features of the systems investigated as compared to the *Y-Si-Al-O-N* system were discovered. Unlike the *Y*-containing system where *J*-phase or woehlerite ($Y_4Si_2O_7N_2$) forms a continuous solid solution with *YAM* ($Y_4Al_2O_9$) neither in *Sm*- nor in *Nd*- containing system the formation of such solid solutions was observed, although the *J*-phase itself was readily formed. The *N*-melilite solid solution *M'(R)* was found to be compatible with *β–SiAlON* phase only in the range β_0–β_{10}. Moreover, according to the *XRD* data *Nd*- and *Sm*- melilite (Ln_2O_3–Si_3N_4) seems to have priority ever β–Si_3N_4 in accommodating *Al* and *O* (thereby forming *M'(R)* phase) and therefore the tie lines between melilite and *β–SiAlON* do not run parallel. The tie line between *β–*Si_3N_4 and $SmAlO_3$ was proven not to exist on account of the results of heat treatment of a number of relevant compositions at 1350 and 1550 ^{0}C that resulted in formation of *M'* and apatite ($Sm_{10}(SiO_4)_6N_2$) only. Graphically these results are presented in Fig. 12-16.

In the *Dy-Si-Al-O-N* system the region defined by the four end-members Si_3N_4, *AlN*, Al_2O_3 and Dy_2O_3, that includes the phases α–*SiAlON*, *β–SiAlON* and *AlN* polytypoids, and covers the range of compositions used for the design and processing of commercial multi-phase sialon ceramics was investigated [53]. The binary tie-lines and 42 compatibility tetrahedra were established based on experimental results and on the more extensive knowledge of phase relationships in the *Y-Si-Al-O-N* and *Sm(Nd)-Si-Al-O-N* systems (Table 6).

The *DyAG* ($Dy_3Al_5O_{12}$) is stable phase and is compatible with all the *AlN* polytypoid phases, β–*SiAlON* (from β_{10} to β_{60}) and α–*SiAlON* (oxygen-rich) forming twelve *Al*–polytypoids- containing compatibility tetrahedra (Fig. 17) and one *α'–β'*–containing

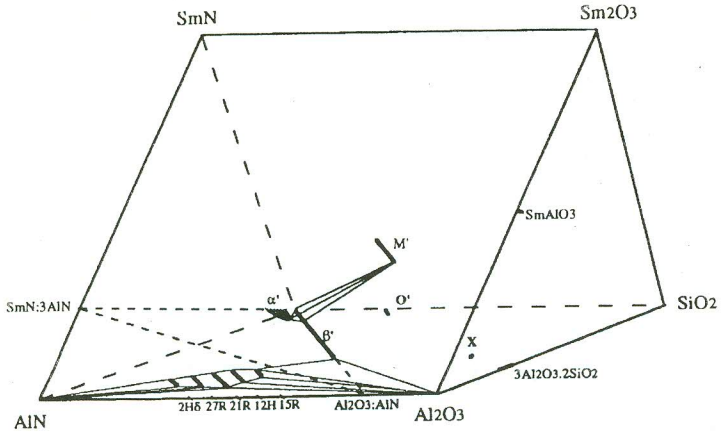

Figure 14: M' (melilite solid solution) is compatible with β–SiAlON ($(\beta_0–\beta_{10})$) and α–SIAlON forming α'–β'–M' compatibility tetrahedron [52].

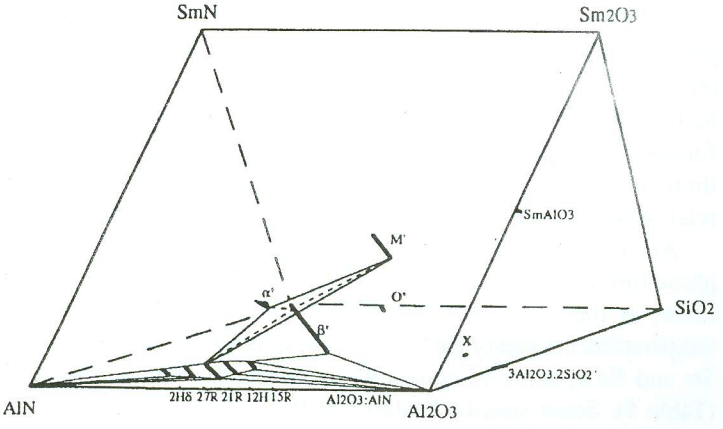

Figure 15: Compatibility tetrahedron α'–β–21R–M' [52].

compatibility tetrahedron, $\alpha'–\beta_{10}–DyAG–12H$ (Fig. 18) unlike the *Sm(Nd)*-containing systems where the *YAG* does not occur. The melilite solid solution *M'* is compatible with both *β*– and *α–SiAlON* phases, and with *DyAG* forming two compatibility tetrahedra: $\alpha'–\beta_0–\beta_{10}–M'$ and $\alpha'–\beta_{10}–M'–DyAG$ (Fig. 19). Moreover, in the *Dy*-containing system the *J*-phase ($Dy_4Si_2O_7N_2$) forms a continuous solid solution with $Dy_4Al_2O_9$ unlike the *Sm(Nd)*-containing ones and similar with *Y* and *Yb* [25, 49, 54]. It was also shown that the compound $DyAlO_3$ is compatible only with *M'* (melilite solid solution) and *Dy*-rich terminals of *AlN* polytypoids (from *AlN* to *21R*), and therefor the tie line between $LnAlO_3$ and *β'* that occurs in the *Nd(Sm)-Si-Al-O-N* systems does not exist in the *Dy-Si-Al-O-N* system. All the results are summarized in Fig. 20.

Subsolidus phase relationships for other *RE*-elements, although not studied in such detail as the ones presented above, could be easily derived by analogy if the *RE*-ionic radius is taken into account appropriately.

Thermal stability of RE-α-SiAlONs and the reversibility of α ↔ β SiAlON transformation

The oxide densification additives used for sintering of *SiAlON* ceramics are generally insoluble in the *β-SiAlON* structure and even though most of them are *α–SiAlON* formers, some additive remains as a residual *M-Si-Al-O-N* intergranular gassy phase, which degrades the mechanical and chemical properties of the material above the glass-softening temperature, which normally is about 900-1100 °C.

Post-sintering heat treatment is one of the accepted methods the main objective of which includes eliminating or minimizing the grain boundary glass in nitrogen ceramics by converting it into refractory crystalline phase(s) thus improving the materials performance at elevated temperatures. This is usually achieved via a conventional glass-ceramic process during which the glass devitrifies at a temperature above its *Tg* point but without being melted [51, 55]. There has been much work in understanding of the grain boundary crystallization, but very little attention has been paid to the effects of the post-sintering heat treatment on the stability of *SiAlON* phases, while the characterization of the finished product has always focused on the account of the residual glass and the type, amount and microstructure of the resulting crystalline oxynitride phase. However, in the course of the study of densification and post sintering heat treatment of *(α–β)-SiAlON* compositions containing selected rare earth oxide additives (Yb_2O_3, Dy_2O_3, Sm_2O_3 either singly or in combination with Y_2O_3) *Mandal et al.* [18] reported that the transformation from *α'* to *β'* readily occurred in some rare earth *α'* + *β'* composite materials when heat treated between 1000 and 1600 °C and that extent of the transformation was more pronounced with increasing temperatures.

α' and *β'* are two different crystallographic modifications of *SiAlON* structures [56]. Although both phases are basically built up of corner sharing $(Si, Al)(O, N)_4$ tetrahedra, there is a distinct difference in the atomic arrangement between the two phases [57]. The transformation between *α'* and *β'* phases has a reconstructive nature, which involves the breaking of chemical bounds and substantial atomic diffusion, and hence requires significant amounts of thermal energy. As a result of the strong covalent nature of the bounding associated with both the *α'* and *β'* structures, the atomic diffusivity of the species making up the lattices is inherently low. It is, therefore, generally assumed that the α'↔ β' phase transformation requires a liquid phase to assist the necessary atomic diffusion by analogy with the transformation from α-Si_3N_4 to β-Si_3N_4, which did not occur without the presence of a liquid phase in which α-Si_3N_4 grains could dissolve above ~1400 °C [58]. However, the actual role of liquid phase in *α'* to *β'* transformation

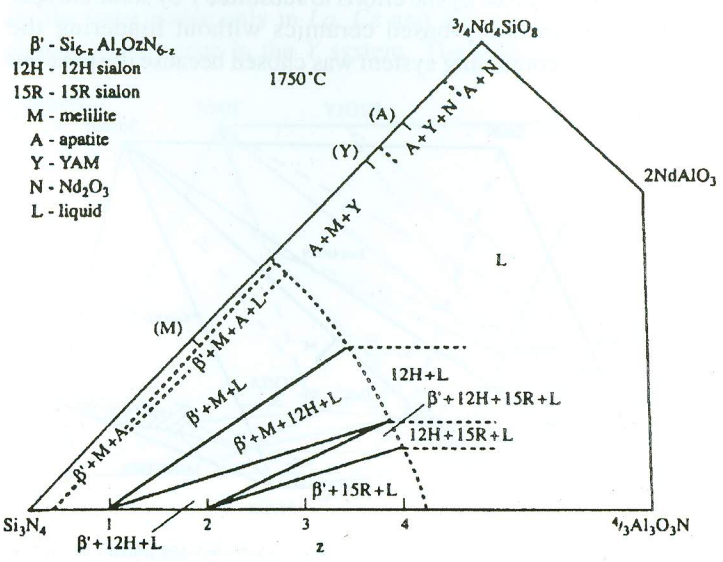

Figure 16: Phase relationships of β'–$NdAlO_3$ plane at 1750 °C [52].

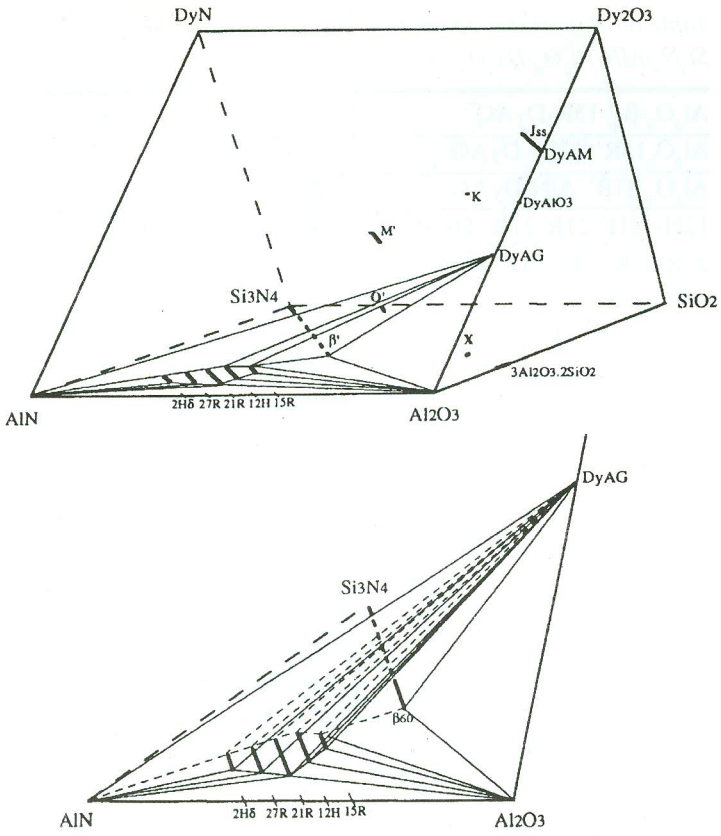

Figure 17: Graphic representation of compatibility of the DyAG with polytypoid phases, AlN, and Al_2O_3, twelve compatibility tetrahedra are formed [53].

has not been fully understood.

According to the observations of [18], the fast cooling (cooling rate of ~ 450 °C/min in the interval 1775-900 °C) of the *RE-SiAlON* samples performed in order to preserve the intergranular phase in a fully amorphous condition led to a marked increase of the α'-phase content. Thus the original samples designated *β-SiAlON* being reheated to the sintering temperature and rapidly cooled contained some α'*-SiAlON*, and the original samples designated *(α–β)-SiAlON* were almost pure *α-SiAlON*. The effect was more marked in the case of samples densified with higher atomic number rare earth oxides. Subsequent annealing of these samples at various temperatures in the range 1000-1800 °C yielded the α' to β' transformation accompanied by crystallization of various secondary phases. Both the extent of the $\alpha' \rightarrow \beta'$ transformation and the resulting secondary phase assembly were obviously dependent on the *RE* oxide used, specifically the ionic radius of the *RE* element. The degree of the $\alpha' \rightarrow \beta'$ transformation was again more pronounced for the higher atomic number rare earth oxide sintering additives.

The dependence of the phase assemblages after heat treatment on the rare earth oxide used is presented in Fig. 21. Therefore, it was concluded that the *α-SiAlON* phase is only stable at high temperatures (typically in excess of 1550 °C) and that it transforms to *β-SiAlON* plus other *Ln*-rich grain boundary phases at lower temperatures.

Further experiments showed that the amount of grain boundary liquid phase in the sample had marked effects on the transformation, and the introduction of an additional amount of glass into a previously stable α' composition could significantly destabilize the

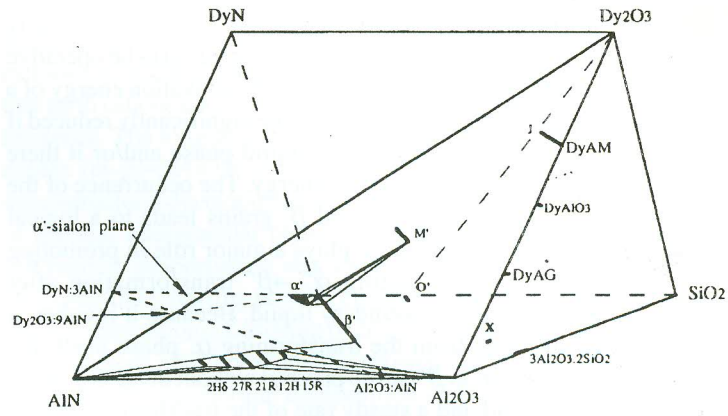

Figure 18: DyAG is compatible with β–SiAlON (β_{10}–β_{60}) and αα'–SiAlON (oxygen-rich) forming α'–β_{10}–12H–DyAG compatibility tetrahedron [53].

α' phase and promote the $\alpha' \rightarrow \beta'$ transformation [21]. After comparing the results in different rare earth *SiAlON* systems, it was further suggested by the same authors that the residual grain boundary liquid phase was one of the most important factors influencing the transformation. The rate of the transformation was stated to be dependent on the amount and viscosity of the intergranular liquid phase present during the heat treatment.

Shen et al. [59] on the other hand, proposed two possible transformation routes, one involving a liquid phase, i.e. α'*+ liquid* $\rightarrow \beta'+M'$ and other being a direct decomposition of the α' phase to form β' and the aluminum-containing melilite ($Sm_2Si_{3-x}Al_xO_{3+x}N_{4-x}$, *M'(R)*) phases in the *Sm* $(\alpha–\beta)$*– SiAlON* system, without the involvement of a liquid phase. However, a more in-depth investigation of the thermal decomposition of samarium and ytterbium stabilized *α–SiAlON* phases revealed that some self-generated liquid phase is involved in the process of $\alpha' \rightarrow \beta'$ transformation [60]. Unique microstructural features resulting from the *α-* to *β-SiAlON* transformation have been observed in *Sm* and *Yb* $(\alpha–\beta)$*-SiAlON* samples. The newly formed β'-grains, namely the ones formed as a result of $\alpha' \rightarrow \beta'$ transformation, contain a high density of dislocations and a large amount of ultra-fine (~40 *nm*) spherical inclusions which are often associated with dislocations. The conclusion that such microstructure is a unique feature associated with the α' to β' transformation was based on careful structural analyses by several methods. It was also shown that the transformed grains grow as a result of the epitaxial heterogeneous nucleation on the pre-existing β'-phase.

According to [61], the $\alpha' \rightarrow \beta'$ transformation occurs in two stages. The first stage involves relatively high amounts of intergranular glassy phase, which provides the liquid phase necessary for transformation since the post-sintering heat treatment is conducted at the temperatures exceeding the melting point of the glass. At this stage the transformation occurs according to the mechanism described in [59]. After the initial period of heat treatment, the volume percentage of the residual grain boundary glass is reduced dramatically; hence its role in the transformation would be severely restricted. Moreover, the *M'* phase formed during the first stage is very stable at the annealing temperatures that have been applied (1450 °C). Once it has formed it would not re-melt to become a grain boundary liquid phase and to be involved in $\alpha' \rightarrow \beta'$ transformation at this temperature [41, 59]. The rate of the $\alpha' \rightarrow \beta'$ transformation at the second stage, i.e. after devitrification of the intergranular glass was accomplished, was observed to be somewhat

lower than at the first stage but the process continued at a nearly constant rate, suggesting an additional mechanism(s) to be operative until the system is closed to equilibrium. The activation energy of a reconstructive phase transformation will be significantly reduced if the atomic diffusion is assisted by a liquid phase and/or it there exist nuclei to reduce the interfacial energy. The occurrence of the self-generated liquid in transformed β' grains leads to a logical assumption that this liquid phase plays a major role in promoting atomic diffusion and facilitating $\alpha''\rightarrow\beta''$ transformation after crystallization of the grain boundary liquid. Because it involves a liquid phase emerging from the transforming α' phase itself, the transformation from α' to β' can be proceed without involving much grain boundary liquid and a steady rate of the transformation may be expected.

The appearance of the *RE*-rich spheroids in the β' phase results in thermodynamic instability, hence these nano-sized inclusions would eventually diffuse out of the transformed β' grains through the easy path of dislocations. It is therefore, suggested in [61] that the amount and viscosity of the self-generated liquid within the transforming α' grains is a determining factor in controlling the rate of the $\alpha'\rightarrow\beta'$ transformation when most at the grain boundary glass has been crystallized.

Without much involvement of grain boundary glass, the $\alpha'\rightarrow\beta'$ transformation at the second stage may be regarded as a decomposition process of *α-SiAlON* phases. This suggests that, below a certain temperature, some of the α' compositions have a higher free energy than β' phases, and the transformation from α' to β' would occur if it could be thermally activated. Because of the compositional difference between α' and β' phases, the decomposition of an α' phase must produce other phases(s) in addition to a β' composition. If in the [59] it was suggested that α' decomposes with the formation of α' and *M'(R)*, the more recent investigations in the *Sm-Si-Al-O-N* system [61] where the EDS X-ray mapping technique was applied for quantification of *AlN* polytypoid phases showed that another, more complicated, reaction path seems to be more plausible for description of *Sm α'–SiAlON* phases decomposition, namely

$$\alpha' \xrightarrow{\text{internal liquid}} \beta' + M' + 21\,R \cdot$$

Further attempts to reach even more complete understanding of the mechanism of this interesting transformation together with the

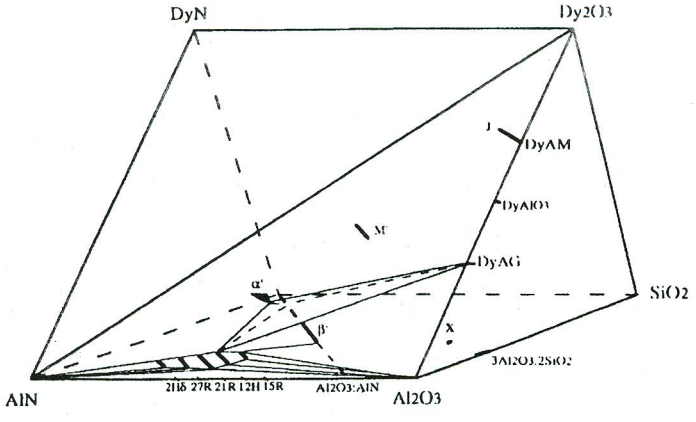

Figure 19: M' (melilite solid solution) is compatible with β–SiAlON (β_0–β_{10}) and α–SiAlON forming α'–β'–M' compatibility tetrahedron [53].

Table 6 - Subsolidus compatibility tetrahedra in the system Si_3N_4-AlN-Al_2O_3-Dy_2O_3 [53].

Al_2O_3-β_{60}-15R-DyAG	Al_2O_3-15R-15R'-DyAG
$Al_2O_3$15R'-12H'-DyAG	Al_2O_3-12H'-21R'-DyAG
Al_2O_3-21R'-AlN-DyAG	15R-15R'-12H-12H'-DyAG
12H-12H'-21R-21R'-DyAG	21R-21R'-27R-27R'-DyAG
27R-27R'-2H$^{\delta}$-2H$^{\delta'}$-DyAG	2H-2H$^{\delta}$-AlN-DyAG
21R'-27R'-AlN-DyAG	27R'-2H$^{\delta'}$-AlN-DyAG
β_{60}-β_{25}-15R-DyAG	β_{25}-15R-12H-DyAG
β_{25}-β_{10}-12H-DyAG	β_{10}-12H-21R-α'
21R-β_{10}-β_8-α'	β_8-21R-27R-α'
27R-β_8-β_5-α'	β_5-27R-2H$^{\delta}$-α'
2H$^{\delta}$-β_5-β_2-α'	β_2-2H$^{\delta}$-AlN-α'
AlN-β_2-β_0-α'	β_0-β_{10}-α'-M'
β_{10}-12H-α'-DyAG	12H-21R-α'-DyAG
21R-27R-α'-M'	27R-2H$^{\delta}$-α'-M'
2H$^{\delta'}$-AlN-α'-M'	AlN-2H$^{\delta}$-M'-DyAP
2H$^{\delta'}$-27R-M'-DyAP	27R-21R-M'-DyAP
AlN- 2H$^{\delta'}$-DyAP-DyAM	2H$^{\delta}$-27R-DyAP-DyAG
27R-21R-DyAP-DyAG	21R-M'-DyAG-DyAP
21R-α'-M'-DyAG	α'-β_{10}-DyAG-M'
J'(middle)-DyAM-DyAP-AlN	Dy_2O_3-J'(whole)-AlN
J-J'(middle)-M-M'-AlN	J'(middle)-M'-DyAP- AlN

DyAM = $Dy_4Al_2O_9$; DyAP = $DyAlO_3$; DyAG = $Dy_3Al_5O_{12}$; 15R, 12H, 21R, 27R, 2H$^{\delta}$ are Si-rich terminals of AlN polytypoids; 15R', 12H', 21R', 27R', 2H$^{\delta'}$ are Al-rich terminals of AlN polytypoids.

evaluation of different rare-earth-doped duplex *(α–β)–SiAlONs* for long term high temperature stability are presented in [62, 63]. Both aspects are of special interest since many applications for *(α–β)–SiAlON* ceramics are in the temperature range where the $\alpha'\rightarrow\beta'$ transformation will continue with consequent continuous change in properties. The research accomplished in [62] was mostly aimed at elucidation of the effect of starting composition, type of rare earth sintering additive and amount of liquid phase on the $\alpha\leftrightarrow\beta$ transformation during post sintering heat treatment. Therefore, five different *(α–β)–SiAlON* and *α–SiAlON* compositions have been prepared using neodymium, samarium, dysprosium and ytterbium. The reasons for preparation of these compositions were as follows:

-first group was formulated as the original starting composition used in [18] and has been shown to readily undergo $\alpha\leftrightarrow\beta$ *SiAlON* transformation;

-the second group was formulated to produce the phase composition ≈ 30% *α–SiAlON* and 70% *β–SiAlON* ;

-the third was also aimed for the two-phase region but was more *α–SiAlON* rich (≈ 50% *α–SiAlON* and 50% *β–SiAlON*); this composition was useful for comparison with the first two compositions to understand the effect of liquid phase, since the amount of liquid is less and the viscosity is higher than in the other two;

-the fourth group was formulated for an *α–SiAlON* with $m = 1$ and $n = 1.7$ (oxygen-rich corner of the *α–SiAlON* phase region) and was designed to determine whether all different cation size rare earth oxide sintering additives give pure *α–SiAlON*, since the borders

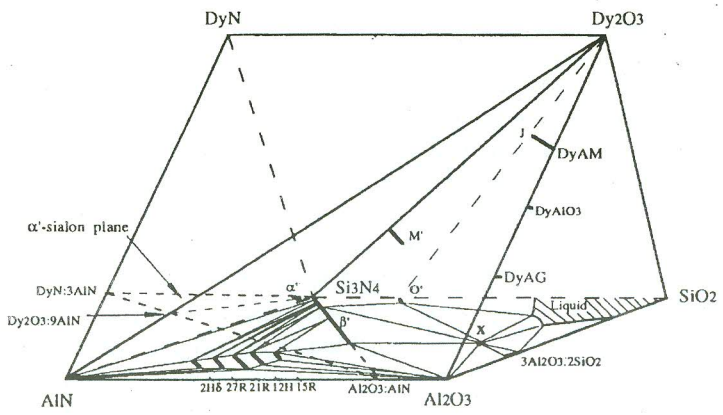

Figure 20: Representation of Dy-Si-Al-O-N system showing phases occurring in the region bound by Si_3N_4, Dy_2O_3, Al_2O_3, and AlN, and Si-Al-O-N behavior diagram at 1700 °C (α–SiAlON plane = the plane with α–SiAlON composition ($Dy_xSi_{12-(m+n)}Al_{m+n}O_nN_{16-n}$) [53].

of α–sialon phase field have only been established precisely in the yttrium system;

-the fifth group was designed as an *α–SiAlON* composition with $m = 1.5$ and $n = 1.5$, representing the maximum nitrogen content α–sialon composition which can be prepared without *LnN*.

A combination of extensive X-ray and microstructural observations on sintered and heat treated samples showed that the *α–SiAlON* composition in mixed *(α–β)–SiAlON* materials is always located at the edge of the *α–SiAlON* phase region and is less stable with respect to *α–β–SiAlON* transformation than in single phase *α–SiAlON* phase region. For *(α–β)–SiAlON* composites the transformation was shown to proceed more readily with the increase of the amount and the decrease of the viscosity of liquid phase formed during heat treatment. For the *α–SiAlON* starting compositions prepared both within or the edge of the *α–SiAlON* phase region, the regularities of the ease of phase transformation are of a more complex nature. A combination of thee factors influences the ease of transformation: the cation size of the sintering additive, the presence of *β–SiAlON* grains and also the amount and viscosity of liquid phase present during heat treatment. The role of the liquid phase in the phase transformation for all compositions was elucidated in the same way: an extra amount (10% and 20%) of glass powders of overall composition *Ln: Si: Al = 1:1:1* to the samples. Such additions led to unequivocal intensification of the $\alpha' \rightarrow \beta$, transformation in all samples with the exception of the ones from the fifth group, that were doped with small ionic size of sintering additives (Dy_2O_3 and Yb_2O_3). For these materials the presence of *β–SiAlON* grains was necessary for triggering the transformation. Moreover, the increase of the number of such grains (10% *β–SiAlON* with $z = 0.8$ was added to one of the mixtures) enhanced the transformation substantially, while such grains might possibly act as a nucleation site for $\alpha \rightarrow \beta$ *SiAlON* transformation. Only then the amount and viscosity of liquid became important factors for the overall reaction *α–SiAlON + β–SiAlON + (21R) + liquid → β–SiAlON + (21R) + grain-boundary phase(s).* *β–SiAlON* nucleation sites provided more favorable kinetic conditions for transformation in case of large ionic size sintering additives, but the process itself proceeded without any additional ones. The overall results are summarized in Table 7, where increasing number of "+" marks indicate the more dominant mechanism influencing $\alpha \leftrightarrow \beta$ *SiAlON* transformation.

Somewhat similar research was carried out for duplex *α–β–SiAlON* stabilized with *Nd*, *Yb* and *Y*. The former two *RE* elements were chosen because they represent the size end members of rare earth cations known to stabilize the *α'*–phase, while *Y* served as a reference. The long-term high-temperature stability of the different duplex *(α–β)–SiAlON* ceramics was of special interest. Phase and microstructural development and the volume fraction and chemistry of residual intergranular phases were characterized and related to mechanical properties. It was shown that on sintering the duplex *(α–β)–SiAlON* starting powder compositions result in equilibrium phase compositions consisting of *α'*, *β'* and a residual glassy phase. The analytical XRD investigations showed that *α'* and *β'* substitution levels and the equilibrium composition and volume fraction of the glass are dependent upon the starting composition as well as the *α'* stabilizing cation. However, the *β'/(α'+β')* weight ratio was shown to depend mostly on the *RE* stability element used. The long-term heat treatment experiments at 1450 °C clearly indicate that *Y* and *Yb* give a stable *α–SiAlON* phase, while *Nd* gives a less stable one that during prolonged heat treatment at 1450 °C decomposes into crystalline phases: melilite, *β–SiAlON*, and *21R* polytypoid. These observations are fully consistent with the results of [62]. Overall, the above described experimental results on *α'*-phase stability and $\alpha \leftrightarrow \beta$ *SiAlON* transformations strongly indicate that for duplex *(α–β)–SiAlON* composites designed for high-temperature applications *RE* elements with smaller ionic radii present an optimal choice.

Reaction densification of α– and (α–β)– SiAlONs

In the previous parts of the present review the importance of proper choice of initial composition, of the type of *RE*-oxide used as a sintering additive and of some processing parameters for optimal phase assemblage formation, and hence of the desired properties of *SiAlONs* were discussed. However, an even more important issue is to achieve the complete densification of *SiAlON* materials, preferably by means of pressure-less sintering. In order to optimize this process basic understanding of the densification behavior of *SiAlONs* is necessary.

Densification of *SiAlONs* occurs by reaction liquid-phase sintering or "transient liquid sintering", the latter concept specifically applied to *SiAlONs*. Intensive investigations have been done on the reaction sintering of *SiAlON* in the *metal oxide-Si_3N_4-AlN-SiO_2-Al_2O_3* system [64-75]. Some of the earliest work was carried out in the *MgO-Si_3N_4-AlN-SiO_2-Al_2O_3* system [64-67]. It was found that a transient phase, which formed during the hot pressing of *α-Si_3N_4* with *MgO*, reacted with *α-Si_3N_4* above 1400 °C to form *β-Si_3N_4* and a vitreous phase [64]. This reaction was found to expedite the sintering kinetics and the reaction pathway of a mixture of *MgO-Si_3N_4-AlN-SiO_2-Al_2O_3* depended on the amount of *MgO* added [64-66]. The addition of Y_2O_3, instead *MgO* to a *Si_3N_4-AlN-SiO_2* mixture resulted in a material with diphasic *β'-SiAlON-$Y_3Al_5O_{12}$* (*YAG*) microstructure with improved mechanical properties [67]. Later the attempts were made to obtain dense *β-SiAlON* ceramics in the *Si_3N_4-AlN-SiO_2-Al_2O_3* plane [68-70]. In these studies, it was shown that the sintering kinetics depended on the composition of starting powder mixtures, even though the final composition was the same. In these and other reaction sintering and hot-pressing studies, the densification mechanisms were identified to be solution-reprecipitation [64-67], fast particle rearrangement [73], Cobble creep [73], or grain boundary sliding [72, 74].

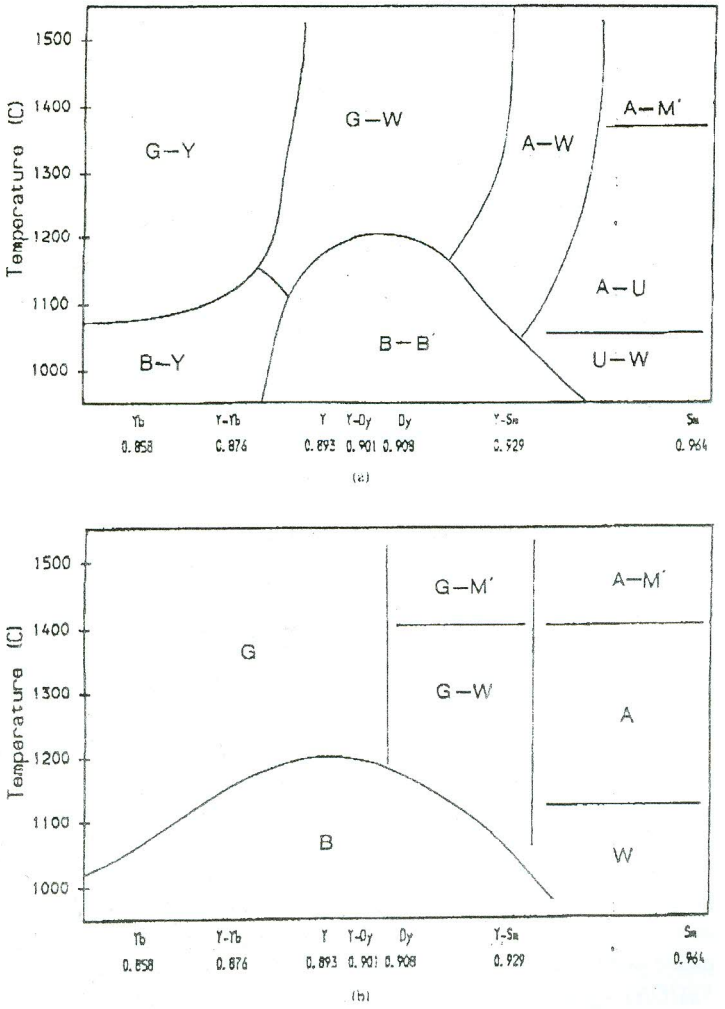

Figure 21: Heat treatment of 1775 °C pressureless sintered (a) β–SiAlON and (b) (α–β)–SiAlON materials. B, B-phase {(Y, Ln)$_2$SiAlO$_5$N}; W, wollastonite {(Y, Ln)SiO$_2$N}; U, U-phase {Ln$_3$Si$_3$Al$_3$O$_{12}$N$_2$}; Y, J(R)-phase {(Y< Ln)Si$_2$O$_2$N$_2$}; G, garnet {(Y, Ln)$_3$Al$_5$O$_{12}$}; A, aluminate {LnAlO$_3$}; and M', melilite {Ln$_2$Si$_3$O$_3$N$_4$}; with some substitution of Si and N by Al and O [18].

Recently, it was shown by *Hwang* and *Chen* that reaction hot pressing of α'- and α'+ β'-*Y-SiAlON* took place in three stages [75]. Further, it was found out that the wetting properties of the Y_2O_3-Al_2O_3-SiO_2 eutectic melt controlled the densification behavior of the powder compact. The first stage was identified with the formation of the ternary oxide eutectic and *YAG*. The shrinkage in this stage was due to the redistribution of liquid in the powder compact and slight improvement in the packing efficiencies. The second stage was identified with the wetting of *AlN* particle and formation of β_{60}. The preferential wetting of *AlN* by the ternary oxide melt caused localization of the liquid, leading to a delaying effect on the second shrinkage step. The third stage occurred with the dissolution of Si_3N_4 and formation of the final phase. Massive particle rearrangement was found to be the dominant densification mechanism. It also caused *Al* enrichment in the liquid, leading to formation of β_{60} as a transient phase. Thus the physical/chemical characteristics of the liquid, in particular its wetting behavior, and the kinetic pathway of the intermediate reactions are clearly important factors in reaction densification of multicomponent systems.

A survey of the literature indicates that until recent time there was almost no knowledge of the wetting characteristics of various ternary oxide eutectic melts on nitrides. Most studies on reaction sintering have been restricted to the documenting of phase evolution and densities. Only limited information may be gleaned from the reports of transient/intermediate phases of these studies. The reaction sequence were studied in *Ca-*, *Y-* and *Nd-α–SiAlON*, and, according to [76, 77], gehlenite ($Ca_2Al_2SiO_7$) was found to be transient phase in *Ca-α– SiAlON*, whereas *N*-melilite ($R_2Si_2O_3N_4$) formed during the densification of *Y-* and *Nd-α– SiAlON*. *N*-melilite was also reported to be a transient phase in *Nd-* and *Sm*-doped *α– SiAlON* [79]. The same phase was identified as a transient one during the pressureless sintering of lanthanide (*Y* and *Nd* to *Ln*, except *Pm*) – modified *α-SiAlON* [80]. *K*-phase ($RSiO_2N$) and β-Si_3N_4 phase along with melilite were determined in the case of *Nd-α–SiAlON* in [31]. Furthermore, in the same work *J*-phase ($R_4Si_2O_2N$) and β-Si_3N_4 were reported to occur along with melilite in the case of *Sm-* and *Gd-α–SiAlON*, and *J* and β-Si_3N_4 in case of *Dy-*, *Y-*, *Er-* and *Yb-α–SiAlON*. The reaction sequence in hot-isostatic-pressed and pressureless-sintered, rare-earth-doped *(α–β)–– SiAlONs* have been studied in [6, 80-83]. Formation of 12*H* and *La*-silicon-oxynitride as the transient phase in the case of *Y-* or *Y/La*-doped samples were reported. Generally it has not been known what controls the formation and selection of various phases. The first indication that a general understanding of reaction sequence during sintering of *SiAlON* materials may, after all, be based on simple physical chemical considerations governing surface activities of nitrides with reactive liquids was given in [75]. There it was shown that in *Y-SiAlON* system, Y_2O_3-Al_2O_3-SiO_2 melt preferentially wets *AlN*, leading to the formation of β_{60}-*SiAlON* as a transient phase, which delays densification in the early stages due to liquid trapping.

A more systematic research of the wetting behavior of the ternary eutectic melt M_2O_3-Al_2O_3-SiO_2 and its interrelation with phase development during reaction hot pressing of α-Si_3N_4, *AlN*, Al_2O_3, and M_2O_3 powder mixtures (*M = Li, Mg, Ca, Y, Nd, Sm, Gd, Dy, Er,* and *Yb*) was accomplished in [84], and in [85] these results were tied in with densification. The evolution of phases on heating was studied by means of heating up the mixtures to some intermediate temperatures, cooling down, and subsequent XRD characterization. The wetting experiments were to study the trends in the wetting behavior of the ternary oxide melts on the nitrides. For this propose ternary eutectic compositions were prepared and pressed into pellets, which were placed on substrates prepared from Si_3N_4 and *AlN* by hot pressing without additives. These "sandwiches" were then heated to different temperatures, in a nitrogen atmosphere, where the pellets fused. On cooling, the contact angles were measured from photomicrographs. Since the wetting characteristics are sensitive to the composition (including the oxygen/nitrogen content in the melt) and the temperature, the true equilibrium was not achieved during the experiments [84]. Therefore, these experiments can not be considered as yielding the actual values of the wetting angle. Lather, an insight into preferential wetting of the nitride powders by the ternary oxide melt in a multicomponent system was provided.

It was shown that the wetting behavior of the ternary oxide melt towards Si_3N_4 and *AlN* was strikingly different, depending on the metal oxide used. Such a preference in reaction sequence was

Table 7 - Mechanisms influencing α↔β SiAlON transformation [62].

Sample (%)	O : N ratio	Sintering additive	α→β SiAlON transformation	Driving force		
				Ln cation size liquid phase	Amount and viscosity of sites	β–SiAlON nucleation
Ln 1	13.7	Nd_2O_3 or Sm_2O_3	+	+++	++	+
		Dy_2O_3 or Yb_2O_3	+	No	+++	+
Ln 2	10.6	Nd_2O_3 or Sm_2O_3	+	+++	++	+
		Dy_2O_3 or Yb_2O_3	+	No	+++	+
Ln 3	9.12	Nd_2O_3 or Sm_2O_3	+	+++	++	+
		Dy_2O_3 or Yb_2O_3	+	No	+++	+
Ln 4	11.88	Nd_2O_3 or Sm_2O_3	+	+++	++	+
		Dy_2O_3 or Yb_2O_3	+	No	++	+++
Ln 5	10.34	Nd_2O_3 or Sm_2O_3	+	+++	++	NO
		Dy_2O_3 or Yb_2O_3	NO	No	NO	+++

explained in [84] in terms of acid-base chemistry. According to the Pearson's principle, hard acids preferentially react with soft bases [40]. Empirically, polarizability, electronegativity, and charge to size ratio [40] can be used as a measure of hardness of as acid or a base [86]. Recently, a model of pH_0 (the point of zero charge that corresponds to the *pH* at which the immersed solid has a zero net surface charge) values calculation for ionic metal oxides based on the ionizational potential of the metal ion was proposed [87]. If the oxides used in [84] are put in order of decreasing basicity according to this model, and if the acidity of the nitrides is assumed to be determined by the acidity of their native oxide layers (in the case Si_3N_4 will be more acidic than *AlN*), than both the experimental wetting data and the sequence of the intermediate reaction products in relation to their *Si/Al* ratio will be in total accordance with the above mention acid-base principle. Therefore, the harder acid, Si_3N_4, reacts with hard bases of oxide melts of *Li*, *Ca*, *Mg*, and lighter rare earth metals up to *Gd*, whereas the soft acid *AlN* reacts with the soft bases of the heavier rare-earth metals down to *Dy*. In the order of decreasing *Si/Al* ratio and additive basicity, typical intermediate phases are *O'* (SiN_2O_2), *M*-cordierite ($Mg_2Al_4Si_5O_{18}$), *M'* ($R_2Si_2AlO_4N_3$), and β_{60}-*SiAlON* ($Si_{0.8}Al_{4.2}O_{4.2}N_{3.8}$).

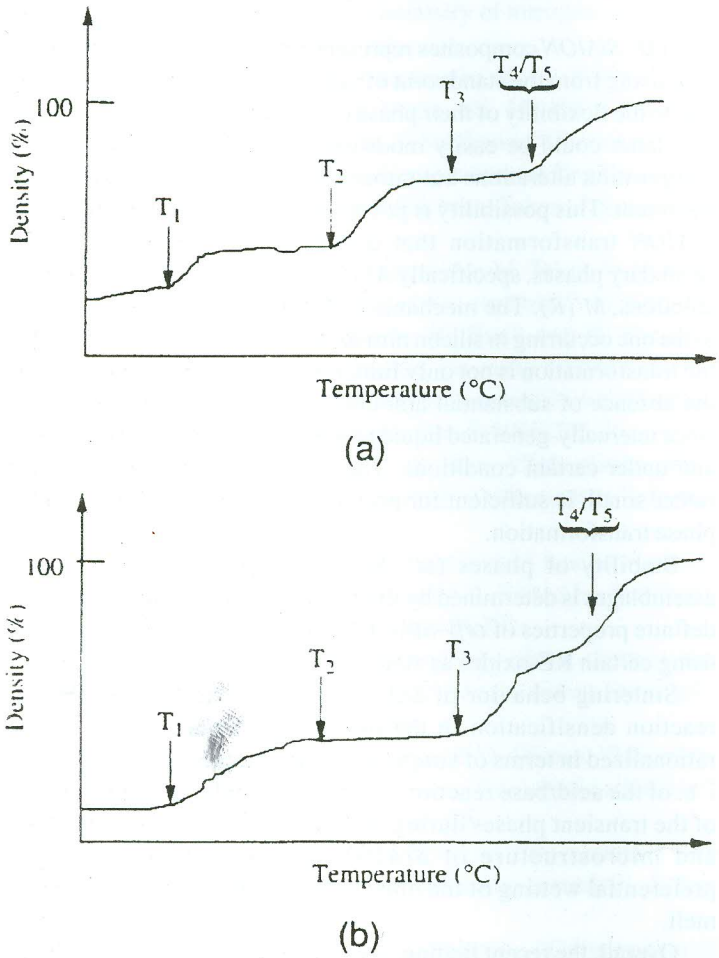

Figure 22: Schematic shrinkage curves when the eutectic melt wets (a) Si_3N_4 and (b) AlN first [85].

The temperatures for the various reactions, which can be used to understand the shrinkage behavior, were also identified in [84] based on the observed wetting/reaction behavior. The reactions identified during the reaction densification of α–*SiAlON* are:
(i) the eutectic formation (at temperature T_1),
(ii) wetting of a nitride powder and intermediate phase precipitation (at temperature T_2),
(iii) secondary wetting of the other nitride powder (at temperature T_3),
(iv) dissolution of the intermediate phase (at temperature T_4), and
(v) precipitation of the final phase, α–*SiAlON* (at temperature T_5)

The schematic representation of expected shrinkage curves when the eutectics melt preferentially wets Si_3N_4 and *AlN* are shown in Fig. 22 (a) and (b), respectively. In these curves, the beginning of various shrinkage steps are identified with some of the above characteristic temperatures. Wetting of *AlN* is shown to lead to small or no immediate shrinkage in the powder compact because of the low *AlN* content of the typical *SiAlON* compact [75]. As it is shown in Fig. 22 (b), though, a subsequent shrinkage step occurs when the majority Si_3N_4 is wetted. Variation of these shrinkage curves may also be possible. For example, it is known that the initial precipitation

Table 8 - Summary of features of the shrinkage curves for samples hot pressed at a heating rate of 15 °C/min [85].

System	T_1(°C)	T_2(°C)	T_3(°C)	T_4(°C)	T_5(°C)	Volume shrinkage	
						First stage	Second stage
Li	1010	1225	1600	1500	1420	8.0	15.0
Ca	1360	1450	1660	1610	1550	5.0	28.0
Mg	1350	1500	1630	>1850	1575	5.0	9.0
Nd	1400	1450	1580	~1800	1420	4.0	15.0
Sm	1380	1460	1600	~1800	1420	7.0	17.0
Gd	1370	1500	1620	1700	1575	7.0	10.0
Dy	1360	~1500	1560		1575/1675	5.0	20
Er	1400	~1500	1580	1640	1580	4.0	13.0
Yb	1380	~1500	1560	1640	1560	9.0	10.0

of the intermediate phase usually starts with partial wetting of the first nitride, i.e., T_2 could be significantly lower than the temperature when complete wetting is achieved. Also, the dissolution of intermediate phase may or may not be higher than T_5. Indeed T_4 may even be lower than T_3, as in case of *Li* and *Ca*, where wetting and dissolution of the second nitride (*AlN*) occurs after the intermediate phase (*O'*) is dissolved and partial formation of *α–SiAlON* is already achieved [85]. Experimental data on the characteristic temperatures of shrinkage determined in [85] for a number of systems are presented in Table 8. Experimental shrinkage curves obtained by means of hot pressing with a constant treating rate [84] were in good agreement with the ones, predicted by the sequence of wetting reactions.

Reaction densification of *M-SiAlON* occurs in three stages. The first stage is associated with the formation of the SiO_2-Al_2O_3-M_2O_3 ternary eutectic (at temperature T_1). The second stage is associated with the preferential wetting of majority nitride powder, Si_3N_4. This occurs at T_2 when Si_3N_4 is wetted first. If *AlN* is wetted first, then no shrinkage step is observed at T_2 and the densification is delayed until T_3, when Si_3N_4 is wetted finally.

The third stage involves the dissolution/melting of the intermediate phase (at temperature T_4) if T_4 is low; otherwise a distinct third stage is not seen while a gradual densification continues following the second stage. In the extreme case of very high T_4, this may result in poor density as in case of *Mg*, where cordierite precipitates as an intermediate phase.

The formation temperature of the final α–*SiAlON* phase (T_5) is not crucial in most cases, unless a sudden secondary precipitation of α–*SiAlON* at this later stage (T'_5) drains the liquid and retards densification. Such material must be densified at temperatures below T'_5. To achieve full densification at relatively low temperatures, a low wetting temperature for the second nitride (T_3) and low dissolution/melting temperature of the intermediate phase (T_4) are required. The dominant process for densification in *SiAlON* ceramics was shown to be massive particle rearrangement although some dissolution facilities full densification by providing the necessary liquid [85].

More generally, the amount of liquid is controlled by the phase diagram, dissolution/melting of intermediate phase, distribution of liquid and secondary precipitation of α–*SiAlON*. The effect of viscosity of liquid as opposite to the most of expectations, is relatively insignificant. The different characteristic temperatures that vary widely among the *SiAlON* systems obscure its effect in most cases. For example, according to [85], although in heavier rare-earth *SiAlONs* in isothermal hot pressing the densification time increased slightly in the order of *Dy*, *Er*, and *Yb*, most probably due to the influence of viscosity, the densification kinetics in constant heating rate do not reflect the same trend, because of non-monotonic variation of characteristic temperatures.

CONCLUSIONS

α/β–SiAlON composites represent a family of ceramic materials promising from the standpoint of tailoring for specific applications due to the flexibility of their phase composition and microstructure. The latter could be easily modified not only by means of initial composition alterations but rather by means of post-sintering heat treatment. This possibility is provided by the fully reversible α↔β *SiAlON* transformation that occurs in the presence of some secondary phases, specifically *Al*-containing nitrogen melilite solid solutions, *M'(R)*. The mechanism of this transformation is similar to the one occurring in silicon nitride, however in the case of *SiAlONs* the transformation is not only fully reversible but also may occur in the absence of substantial amounts of intergranular liquid phase since internally-generated liquid phase forms at certain temperatures and under certain conditions. The amount of the latter, although rather small, is sufficient for promoting the reconstructive α'↔β' phase transformation.

Stability of phases (*α'*, *M'(R)*, *J'(R)*, etc.) and of phase assemblages is determined by the rare-earth ionic radius. Therefore, definite properties of *α/β–SiAlON* composites may be achieved by using certain RE-oxides as sintering additives.

Sintering behavior of *SiAlONs*, which can be described as reaction densification in the presence of liquid phase, can be rationalized in terms of simple physical chemical considerations, i. e. of the acid/base reaction principle. Shrinkage and formation of the transient phases during sintering as well as the final phase and microstructure of *SiAlON* ceramics depends on the preferential wetting of the nitrides by the *RE*-containing silicate melt.

Overall, the recent findings indicate that a good basis for further *SiAlON* development has been achieved due to diverse in-depth research of a variety of *RE-Si-Al-O-N* systems.

ACKNOWLEDGEMENTS

The financial support of the research activities of Dr. V. A. Izhevskyi by CNPq during his stay at IPEN as an invited scientist is highly appreciated.

REFERENCES

[1] Y. Oyama, O. Kamigaito, "Solid solubility of some oxides in Si_3N_4", Jpn. J. Appl. Phys. **10**, (1971) 1637-42 .
[2] K. H. Jack, "Solid solubility of alumina in silicon nitride", Trans. J. Brit. Ceram. Soc. **72** (1973) 376-78.
[3] K. H. Jack, W. I. Wilson, "Ceramics based on the Si-Al-O-N and relates systems", Nature Phys. Sci. (London), **238**, (1972) 28-29 .
[4] L. J. Gauckler, H. L. Luckas, G. Petzow, "Contribution to the phase diagram Si_3N_4-AlN-Al_2O_3-SiO_2", J. Am. Ceram. Soc. **58**, (1975) 346 -48.
[5] K. H. Jack, "The significance of structure and phase equilibria in the development of silicon nitride and sialon ceramics", Sci. Ceram. **11**, (1981) 125-42.
[6] T. Ekström, P.-O. Käll, M. Nygren, "P.-O. Olssen. Dense single-phase β-sialon ceramics by glass-encapsulated hot isostatic pressing", J. Mater. Sci. **24**, (1989)1853-61.
[7] Z. K. Huang, W.-Y. Sun, D.-S. Yan, "Phase relations of the Si_3N_4-AlN-CaO system", J. Mater. Sci. Lett. **4**, (1985) 255-59.
[8] S. Hampshire, H. K. Park, D. P. Thompson, K. H. Jack, "α-Sialon ceramics" Nature (London) **274**, (1978) 880-83.
[9] D. P. Thompson, "The crystal chemistry of nitrogen ceramics", Mater. Sci. Forum **47**, (1989) 21-42.
[10] M. Mitomo, H. Tanaka, K. Muramatsu, N. Li, Y. Fujii, "The strength of α-Sialon ceramics", J. Mater. Sci. **15** (1980) 2661-61
[11] M. Mitomo, F. Izumi, Y. Bando, Y. Sakikawa, "Characterization of α-Sialon ceramics", in: Ceramic Components for Engines. Edited by S. Somiya et al. KTK Science Publishers, Tokyo, Japan (1984) 377-86.
[12] K. Ishizawa, N. Ayuzawa, A. Shiranita, M. Takai, N. Uchida, M. Mitomo, "Some properties of α-sialon ceramics", in: Ceramic Components for Engines. Edited by W. Bunk and H. Hausner, German Ceramic Society, Bad Honnet, Germany (1986) 511-18.
[13] D. Stutz, P. Greil, G. Petzow, "Two-dimensional solid solution forming of Y-containing α- Si_3N_4", J. Mater. Sci., Lett. **5** (1986) 335-36.
[14] Z. K. Huang, T. Y. Tien, D. S. Yen, "Subsolidus phase relationship in the Si_3N_4-AlN-Rare Earth oxide systems", J. Am. Ceram. Soc. **69** (1986) C-241-C-242.
[15] M. Mitomo, "In situ microstructure control in silicon nitride based ceramics", in: Advanced Ceramics II. Edited by S. Somiya Elsevier, Barking, Essex. U.K., (1988) 147-61.
[16] T. Ekström., "Effect of composition, phase content and microstructure on the performance of yttrium sialon ceramics", Mater. Sci. Eng. **A109** (1989) 341-49.
[17] T. Ekström, P.-D. Käll, M. Nygren, P. O. Olsson, "Mixed α– and β– (Si-Al-O-N) materials with yttria and neodymia additions", Mater. Sci. Eng. **A105/106**, (1988) 161-65.
[18] H. Mandal, D. P. Thompson, T. Ekström, "Reversible α ↔ β SiAlON transformation in heat-treated sialon ceramics", J. Eur. Ceram. Soc. **12** (1993) 421-429.
[19] H. Mandal, D. P. Thompson, T. Ekström, "Optimization of sialon ceramics by heat treatment", in: Third Euro - Ceramics, Vol. 3, ed. P. Duran and J. F. Fernandez. Faenza Editrice Iberica S.L., Spain (1993) 385-390.
[20] H. Mandal, D. P. Thompson, Y. W. Sun, T. Ekström, "Mechanical property control of rare earth oxide densified α– β", in: 5th International Symposium on Ceramic materials and Components for Engines, ed. D.S. Yan, Y.R. Fu and S.Y. Shi. World Scientific Publishers. Singapore (1995) 441-446.
[21] H. Mandal, D. P. Thompson, "Mechanism of α – β SiAlON transformation", in: Fourth Euro – Ceramics, ed. G. Galus Gruppo Editoriale. Faenza Editrice S.p.A , Faenza, Italy, (1995) 273-280.
[22] Y.-B. Cheng, D. P. Thompson, "Aluminum – containing nitrogen melilite phases", J. Am. Ceram. Soc. **77**, (1994) 143-48.
[23] H. Camuscu, H. Mandal, D. P. Thompson, "Optimized high-temperature sialon ceramics containing melilite as the grain boundary phase", in: 21st Century Ceramics, British Ceramic Proceedings, ed. D. P. Thompson **55,** (1996)239-248.
[24] H. Mandal, Y.-B. Cheng, D. P. Thompson, " α– SiAlON ceramics with a crystalline melilite grain-boundary phase", in: Proceedings of the 5th International Symposium on Ceramic materials and Components for Engines, 1994 Shanghai, ed. D.S. Yan, Y.R. Fu and S.Y. Shi. World Scientific Publishers. Singapore (1995) 202-205.
[25] V. A. Ijevskii, U. Kolitsch, H. J. Seifert, I. Wiedmann, F. Aldinger, " Aluminum- containing Ytterbium Nitrogen Woehlerite solid solutions. Synthesis, Structure and some properties", J. Eur. Ceram. Soc. **18** (1998) 543-52.
[26] K. H. Jack, "Fabrication of dense nitrogen ceramics", in: Processing of Crystalline Ceramics. Ed. By H. Palmour III, R. F. Davis and T. M. Hane. Plenum Press, New York (1978) 561-78.
[27] R. Marchand, A. Jayaweera, P. Verdier, J. Lang, "Preparation and characterization of new oxynitrides in the lanthanide-sialon-oxide-nitride system", Acad. Sci. Paris **C. R. 283**, (1976) 675-77.
[28] K. H. Jack, "Silicon Nitride Sialons and related ceramics", in Ceramics and Civilization, vol. III, High-Technology ceramics. American ceramic Society, Columbus, OH (1986) 259-88.
[29] P. L. Wang, H.Y. Tu, W. Y. Sun, D. S. Yan, M. Nygren, T. Ekström, "Study on the solubility of Al in the melilite systems $R_2Si_{3-x}Al_xO_{3+x}N_{4-x}$ with R= Nd, Sm, Gd, Dy and Y", J. Eur. Ceram. Soc. **15** (1995) 689-695.
[30] R. K. Harris, M. J. Leach, D. P. Thompson, "Nitrogen-15 and oxygen-17 NUR spectroscopy of silicates and nitrogen ceramics", Chem. Mater. **4** (1992) 260-267.
[31] P. L. Wang, W. Y. Sun, D. S. Yan, "Formation and densification of R-α'-SiAlONs (R= Nd, Sm, Gd, Dy, Er and Yb)", in: Silicon Nitride Ceramics: Scientific and Technological Advances, vol. 287, Eds. I.-W. Chen, P. F. Becher, M. Mitomo, G. Petzow and T.-S. Yen. Materials Research Society (1993) 387-92.
[32] M. J. Hoffman, G. Petzow, "Microstructural design of Si_3N_4 based ceramics", Ibid., 3-14.
[33] K. S. Chee, Y.-B. Cheng, M. E. Smith, "The solubility of aluminum in Rare Earth Nitrogen Melilite Phases", J. Eur. Ceram. Soc. **15** (1995) 1213-1220.
[34] S. Slasor, K. Liddel, D. P. Thompson, "The role of Nd_2O_3 as an additive in the formation of α'and β' sialons", Br. Ceram. Proc. **37** (1086) 51-64.
[35] P.-O. Käll, T. Ekström, "Sialon ceramics made with mixtures of Y_2O_3-Nd_2O_3 as sintering aids", J. Eur. Ceram. Soc. **6** (1990) 119-127.
[36] B. K. Vainstein, V. M. Fridkin, V.L. Indenbom, "Crystallochemical radu systems", In Modern Crystallography II, Structure of Crystals, Ed. By B. K Veinstein, A. A Chernov and L. A Shuvalov, Springer, Berlin, Heidelberg (1982) 78-81.

[37] G. Z. Cao, R. Metselar, "α- Sialon Ceramics: A Review", Chem. Mater. **3** (1991) 242-53.
[38] Z. K. Huang, S. Y. Liu, A. Rozenflanz, I. W. Chen, "Sialon composites containing rare-earth melilite and neighboring phases", J. Am. Ceram. Soc. **79** (1996) 2081-90.
[39] Z. K. Huang, I. W. Chen, "Rare-earth melilite solid solution and its phase relations with neighboring phases", Ibid. **79** (1996) 2091-97.
[40] J. E. Huheey, "Inorganic Chemistry", Harper and Row. New York, (1983).
[41] Z. K. Huang, D.-S. Yan, T. S. Tien, "Compound formation and melting behavior in the AB compound and rare earth oxide systems", J. Solid State Chem. **85** (1990) 51-55.
[42] I. W. Chen, D. P. Thompson, "Preparation and grain boundary devitrification of samarium α-SiAlON ceramics", J. Eur. Ceram. Soc. **14** (1994) 13-21.
[43] Z. K. Huang, P. Greil, G. Petzow, "Formation of α-Si_3N_4 solid solution in the system Si_3N_4-AlN-Y_2O_3", J. Am. Ceram. Soc. **66** (1983) C-96-C-97.
[44] W. Y. Sun, T. S. Tien, T. S. Yen, "Solid solubility limit of single-phase region of α-SiAlON solid solutions in the system Si, Al, Y/N, O", J. Am. Ceram. Soc. **74** (1991) 2547-50.
[45] W. Y. Sun, T. S. Tien, T. S. Yen, "Subsolidus phase relationships in part of the system Si, Al, Y/N, O: the system Si_3N_4-AlN-YN-Al_2O_3-Y_2O_3", J. Am. Ceram. Soc. **74** (1991) 2753-58.
[46] D. P. Thompson, "Phase relationship in Y-Si-Al-O-N ceramics", in: Proceedings of the 21st. University Conference on Ceramic Science, Tailoring Multiphase and Composite Ceramics, edited by R. E. Tressler et al. Plenum Press, New York, (1986) 79-91.
[47] M. Mitomo, F. Izumi, S. Horiuchi, Y. Matsui, "Phase relationships in the system Si_3N_4-SiO_2-La_2O_3", J. Mater. Sci. **17** (1982) 2359-66.
[48] W. Y. Sun, T. S. Yen, T. S. Tien, "Subsolidus phase relationships in the system RE-Al-O-N (Where R= rare earth elements)", J. Solid State Chem. **95** (1991) 424-29.
[49] W. Y. Sun, Z. K. Huang, T. S. Tien, T. S. Yen, "Phase relationships in the system Y-Al-O-N", Mater. Sci. Lett. **11** (1991) 67-69.
[50] H. Mandal, D. P. Thompson, T. Ekström, "Heat treatment of Ln-Si-Al-O-N glasses", in: Proc. 7th. Irish Mater. Forum Conf. IMF7, Eds. M. Buggy and S. Hampshire. Trans. Tech. Publications, Switzerland, (1992) 187-203.
[51] D. P. Thompson, "New grain-boundary phases for nitrogen ceramics", Mater. Res. Soc., Symp. Proc. **287** (1993) 79-92.
[52] W. Y. Sun, D. S. Yan, L. Gao, H. Mandal, D. P. Thompson, "Subsolidus phase relationships in the systems Ln_2O_3-Si_3N_4-AlN-Al_2O_3 (Ln = Nd, Sm)", J. Eur. Ceram. Soc. **15** (1995) 349-355.
[53] W. Y. Sun, D. S. Yan, L. Gao, H. Mandal, D. P. Thompson, "Subsolidus phase relationships in the systems Dy_2O_3-Si_3N_4-AlN-Al_2O_3", Ibid. **16** (1996) 1277-1282.
[54] U. Kolitsch, V. A. Ijevskii, H. J. Seifert, I. Wiedmann, F. Aldinger, "Formation and general characterization of a previously unknown ytterbium silicate (A-type Yb_2SiO_5)", J. Mater. Sci. **32** (1997) 6135-39.
[55] M. H. Lewis, "Crystallization of grain boundary phases in silicon nitride and SiAlON ceramics", in: Silicon Nitride 93, Key Engineering Materials, Eds. M. J. Hoffmann, P. F. Becker and G. Petzow, Trans. Tech. Pub. **89-91** (1993) 333-38.
[56] K. H. Jack, "Review: SiAlONs and related nitrogen ceramics", J. Mater. Sci. **11** (1976) 1135-58.
[57] S. Hampshire, "Nitride Ceramics", in : Materials Science and technology, Structure and properties of Ceramics, ed. M. Swain, VCH, Weinheim **11** (1994) 121-71.
[58] S. Hampshire, K. H. Jack, "The kinetics of densification and phase transformation of nitrogen ceramics", in: Special Ceramics 7, Proc. Brit. Ceram. Soc., Eds. DW Taylor and P. Popper **31** (1981) 37-49.
[59] Z. Shen, T. Ekström, M. Nygren, "Temperature stability of samarium-doped α- SiAlON ceramics", J. Eur. Ceram. Soc. **16** (1996) 43-54.
[60] R. Zhao, Y. B. Cheng, "Microstructural feature of the α- to β-SiAlON phase transformation", J. Eur. Ceram. Soc. **16** (1996) 529-34.
[61] R. Zhao, Y. B. Cheng, "Decomposition of Sm α-SiAlON phases during post-sintering heat treatment" J. Eur. Ceram. Soc. **16** (1996) 1001-08.
[62] H. Camuscu, D. P. Thompson, H. Mandal, "Effect of starting composition, type or rare earth sintering additive and amount of liquid phase on α ↔ β SiAlON transformation", J. Eur. Ceram. Soc. **17** (1997) 599-613.
[63] L. K. L. Falk, Z. J. Shen, T. Ekström, "Microstructural stability of duplex α – β SiAlON ceramics", J. Eur. Ceram. Soc. **17** (1997) 1099-1112.
[64] P. Drew, M. H. Lewis, "The microstructure of silicon nitride ceramics during hot-pressing transformations", J. Mater. Sci. **9** (1974) 261-69.
[65] M. H. Lewis, B. D. Powell, P. Drew, R. J. Lumby, B. North, A. J. Taylor, "The formation of single-phase Si-Al-O-N ceramics", J. Mater. Sci. **12** (1977) 61-74.
[66] M. H. Lewis, A. R. Bhatti, R. J. Lumby, B. North, "The microstructure of sintered Si-Al-O-N ceramics", J. Mater. Sci. **15** (1980) 103-13.
[67] M. H. Lewis, R. J. Lumby, "Nitrogen ceramics: liquid phase sintering" Powder Metall. **26** (1993) 73-81.
[68] G. K. Layden, "Process development for pressureless sintering of SiAlON ceramic components", Report No. R175-91072-4. United Technologies Research Center, (1976).
[69] S. Boskovich, L. J. Gauckler, G. Petzow, T. Y. Tien, "Reaction sintering forming β-Si_3N_4 solid solution in the system Si, Al / N, O", I: Sintering of Si_3N_4-AlN mixtures. Powder Metall. Int. **9** (1977) 185-89.
[70] S. Boskovich, L. J. Gauckler, G. Petzow, T. Y. Tien, "Reaction sintering forming β-Si_3N_4 solid solution in the system Si, Al / N, O", II: Sintering of Si_3N_4-SiO_2-AlN mixtures. Powder Metall. Int. **10** (1978) 180-85.
[71] S. Boskovich, L. J. Gauckler, G. Petzow, T. Y. Tien, "Reaction sintering forming β-Si_3N_4 solid solution in the system Si, Al / N, O", III: Sintering of Si_3N_4-AlN-Al_2O_3 mixtures. Powder Metall. Int. **11** (1979) 169-71.
[72] M. N. Rahman, F. L. Riley, R. J. Brook, "Mechanisms of densification during reaction hot-pressing in the system Si-Al-O-N", J. Am. Ceram. Soc. **63** (1980) 648-53.
[73] M. Kuwabara, M. Benn, F. L. Riley, "The reaction hot pressing of compositions in the system Al-Si-O-N corresponding to β '– SiAlON", J. Mater. Sci. **15** (1980) 1407-16.
[74] M. Havier, P. L. Hansen, "Hot-pressing and α–β' phase transformation of compositions corresponding to β '– SiAlON", J. Mater. Sci. **25** (1990) 992-96.
[75] S. L. Hwang, I. W. Chen, "Reaction hot pressing of α and β '– SiAlON ceramics", J. Am. Ceram. Soc. **77** (1994) 165-71.
[76] W. Y. Sun, P. A. Walls, D. P. Thompson, "Reaction sequences in preparation of Sialon ceramics", in: Non-Oxide Technical and Engineering Ceramics Proc. Inter. Conf., Limerick, Ireland, 1985, Ed. S. Hampshire. Elsevier Applied Science, London, England, (1986) 105-17.
[77] S. Slasor, D. P. Thompson, "Preparation and characterization of yttrium-α'– SiAlONs", Ibid., 223-30.
[78] S. Hampshire, K. P. J. O'Reilly, M. Leigh, M. Redington, "Formation of α'– SiAlONs with neodymium and samarium

modifying cations", in: High Tech Ceramics. Edited by P. Vincezini. Elsevier Science, Amsterdam, Netherlands, (1987) 933-40.
[79] K. P. J. O'Reilly, M. Redington, S. Hampshire, M. Leigh", Parameters affecting pressureless sintering of α'– SiAlONs with lanthanide modifying cations", in: Silicon Nitride Ceramics Scientific and Technological Advances, Proc. Mat. Res. Soc. Symp. **287** (Boston, MA, Nov. 30- Dec. 3, 1992). Ed. I. W. Chen, P. F. Pedier, M. Mitomo, G. Petzow, and T. S. Yen. . Materials Research Society, Pittsburgh, DA, (1993) 393-98.
[80] T. Ekström, "SiAlON ceramics sintered with yttria and rare earth oxides", Ibid., 121-32.
[81] T. Ekström, P. O. Olssen, " β '– SiAlON ceramics prepared at 1770 °C by hot-isostatic pressing", J. Am. Ceram. Soc. **72** (1989) 1722-24.
[82] T. Ekström, P. O. Olssen, "Pressureless sintering of SiAlON ceramics with mixed Y_2O_3-La_2O_3 additions", J. Mater. Sci., Lett. **6** (1989) 119-27.
[83] T. Ekström, P. O. Olssen, "HP- sintered β– and α–β– SiAlONs densified with Y_2O_3 and La_2O_3 additions", J. Mater. Sci. **25** (1990) 1824-32.
[84] M. Menon, I. W. Chen, "Reaction densification of α'– SiAlON. I: Wetting behavior and acid-base reactions", J. Am. Ceram. Soc. **78** (1995) 545-52.
[85] M. Menon, I. W. Chen, "Reaction densification of α'– SiAlON. II: Densification behavior", Ibid., 553-59.
[86] R. G. Pearson, "Absolute electronegativity and hardness: application to inorganic chemistry", Inorg. Chem. **27** (1988) 734-40.
[87] A. Carre, F. Roger and C. Varinot. Study of acid/base properties of oxide, oxide glass and glass-ceramic surfaces. J. Colloid Interface Sci. **154** (1990) 174-83.
(Rec. 12/98, Ac. 02/99)
(Publicação financiada pela FAPESP)